NUMERICAL MODELING AND SIMULATION OF HOT AIR JET ANTI-ICING SYSTEM EMPLOYING CHANNELS FOR ENHANCED HEAT TRANSFER

BY

KAMRAN ZAKI AHMED

A Thesis Presented to the

DEANSHIP OF GRADUATE STUDIES

KING FAHD UNIVERSITY OF PETROLEUM & MINERALS

DHAHRAN, SAUDI ARABIA

In Partial Fulfillment of the
Requirements for the Degree of

MASTER OF SCIENCE

In

AEROSPACE ENGINEERING

JUMADA AL'THANI 1433

APRIL 2012

KING FAHD UNIVERSITY OF PETROLEUM AND MINERALS

DHAHRAN 31261, SAUDI ARABIA

DEANSHIP OF GRADUATE STUDIES

This thesis, written by **Kamran Zaki Ahmed** under the direction of his thesis advisor and approved by his thesis committee, has been presented to and accepted by the Dean of Graduate Studies, in partial fulfillment of the requirements for the degree of **MASTER OF SCIENCE IN AEROSPACE ENGINEERING.**

Thesis Committee

Dr. Farooq Saeed (Advisor)

Dr. Ahmed Z. Al-Garni (Co-Advisor)

Dr. Wael G. AbdelRehman (Member)

Dr. Edi Prasetyo (Member)

Dr. Mohamed Antar (Member)

Dr. Ahmed Z. Al-Garni
Department Chairman

Dr.Salam A. Zummo
Dean of Graduate Studies

Date 18/6/12

بسم الله الرحمن الرحيم

To

My Beloved Parents

for their

Innumerable prayers, Encouragement &

Motivation.

ACKNOWLEDGMENT

IN THE NAME OF ALLAH, THE MOST BENEFICIENT, THE MOST MERCIFUL

Proclaim! In the name of thy Lord and Cherisher, Who created man, out of a (mere) clot of congealed blood. Proclaim! And thy Lord is Most Bountiful, He who taught (the use of) the pen, taught man that which he knew not. Nay, but man doth transgress all bounds, in that he looketh upon himself as self-sufficient. Verily, to thy Lord is the return (of all). **(**Surah 96: Al 'Alaq, 1-8**)**

All praises belong to Allah (SWT), the Cherisher and Sustainer of the worlds, none is worthy of worship but Him. I am sincerely thankful to Him for His kindest blessings on me and all the members of my family. He was with me in the most difficult of times and always. Peace and blessings of Allah be upon our dearest prophet, Muhammad, his family and his companions.

I am grateful to King Fahd University of Petroleum & Minerals, for providing a great environment for research. I would like to express my profound gratitude and appreciation to my Advisor Dr. Farooq Saeed, for his consistent help, guidance and attention that he devoted throughout the course of this work. Special thanks to his indigenous discussion over FLUENT and GAMBIT.

My sincere and heart-felt thanks to Dr. Ahmed. Z. Al-Garni, my Co-Advisor and Chairman of Aerospace Engineering Department. His valuable suggestions, encouragement and useful discussions made this work interesting to me.

Special and sincere thanks also go to my thesis committee members Dr. Wael G. Abdelrahman, Dr. Edi Prasetyo, and Dr. Mohamed Antar for their interest, cooperation and constructive advice.

I would also like to acknowledge all AE faculty members, who were involved with my M.S course work specially Dr. Ayman Kassem. Their knowledge and experience led me to secure this degree in a very professional manner. I also owe thanks and

recognition to my fellow research assistants, course mates, colleagues and friends for their help, motivation and support. Special thanks to Mr. Mohammed Mumtaz Ahmed Khan for his moral and technical support.

Last but not the least, I humbly offer my sincere thanks to my parents for their incessant inspiration, blessings and prayers. They stood by me in my most difficult of times, and no words of appreciation can fully express my gratitude towards them. I pray to Allah (swt) to give us all Hidayah and Pardon our sins and grant us Paradise. Ameen

TABLE OF CONTENTS

LIST OF TABLES

LIST OF FIGURES

NOMENCLATURE

A	surface area (m^2)
d	slot diameter (m)
E	total energy per unit volume (J/m^3)
e	internal energy (J)
H	distance of jet from impinging plate (m)
h/d	non-dimensional channel height to slot diameter ratio (channel height)
k	thermal conductivity
Nu	Nusselt number = hL/k_f
p	pressure, Pa
Pr	Prandtl number = v/α
Q	heat transfer rate (W)
Q''	heat flux ($Btu/hr\text{-}ft^2$)
R	radius of jet (m)
Re	Reynolds number = $\rho V d/\mu$
s	slot area = 2 × jet diameter (m)
T	temperature, K
T_{in}	hot-air jet inlet temperature (K)
T_{wall}	impingement wall temperature (K)
x	position on impinging plate
x/s	non-dimensional distance measured from stagnation point
z/d	non-dimensional jet inlet to slot diameter ratio (jet-to-target spacing)

Symbols

θ	channel inlet location angle
Φ	specific quantity per unit volume
μ	viscosity (kg/m-s)
μ_{ref}	reference viscosity (kg/m-s)
ρ	density (kg/m^3)
ρ_{ref}	reference density (kg/m^3)

Subscripts

avg	average
in	inlet
out	outlet
ref	reference
wall	impingement wall of the model

THESIS ABSTRACT (ENGLISH)

NAME: KAMRAN ZAKI AHMED

TITLE: NUMERICAL MODELING AND SIMULATION OF HOT AIR JET ANTI-ICING SYSTEM USING CHANNELS FOR ENHANCED HEAT TRANSFER

MAJOR: AEROSPACE ENGINEERING

DATE: APRIL 2012

Aircraft icing is a serious concern for the aviation community since it is one of the major causes of fatal aircraft accidents. Aircrafts use different anti-icing systems and one such system is the hot-air anti-icing system, which utilizes hot-air from the engine compressor bleed to heat critical aircraft surfaces and prevent ice formation. Numerous experimental and numerical studies have been performed to increase the efficiency of the hot-air jet based anti-icing systems. Most of the investigations have focused on either orifice design or the impingement region of target surface geometry. Since the impingement surface heat transfer drops off sharply past the stagnation region, investigators have studied the use of multiple jets to enhance surface heat transfer over a larger area. However, use of multiple jets is a further strain on engine resources. One way to conserve engine resources is to use single jet in conjunction with various geometric and physical mechanisms to enhance heat transfer. The current study focuses on enhancing heat transfer using a single jet and a channel. The study investigates the effect of channel's height, inlet location and Reynolds number on heat transfer characteristics in terms of average Nusselt number distribution along the impingement surface. The commercial CFD code, FLUENT, is used to simulate the different cases. Results indicate that the heat transfer depends strongly on height and width of channel, jet-to-target spacing, inlet angle and jet Reynolds number.

MASTER OF SCIENCE DEGREE
KING FAHD UNIVERSITY OF PETROLEUM AND MINERALS
DHAHRAN, SAUDI ARABIA

THESIS ABSTRACT (ARABIC)

الاسم: قمران زكي أحمد

العنوان: نمذجة ومحاكاة عددية لنفث الهواء الساخن بنظام منع الجليد باستخدام قنوات لتحسين انتقال الحرارة

التخصص: هندسة الطيران والفضاء

التاريخ: أبريل 2012

إن تكون الجليد على الطائرات هو مشكلة خطيرة لمجتمع الطيران لأنه أحد الأسباب الرئيسة لحوادث الطائرات المميتة، تستخدم الطائرات نظماً مختلفة لمنع الجليد من التكون، وأحد هذه النظم هو نظام منع الجليد باستخدام الهواء الساخن، والذي يستخدم هواءً ساخناً من نزف ضاغط المحرك لتسخين أسطح الطائرة المهمة ومنع تكون الجليد عليها، ولقد تم إجراء الكثير من الدراسات التجريبية والعددية لتحسين كفاءة نظم منع الجليد المعتمدة على نفث الهواء الساخن، وركزت أغلب الأبحاث على تصميم بفتحات نفث متعددة، أوعلى منطقة الارتطام من سطح الهدف، ونظراً لأن انتقال الحرارة على سطح الارتطام يقل بشدة بعد منطقة السكون، فإن الباحثين قاموا بدراسة استخدام عدة فوهات نفث لتحسين انتقال الحرارة فوق مساحة أكبر، ولكن استخدام عدة فوهات نفث يضيف عبئاً إضافياً على المحرك، وأحد طرق الحفاظ على موارد المحرك هي استخدام فوهة نفث واحدة مع تركيبات هندسية ومادية لتحسين انتقال الحرارة، تركز الدراسة الحالية على تحسين انتقال الحرارة باستخدام نفث أحادي وقناة، وتبحث الدراسة في تأثير ارتفاع القناة، ومكان الفوهة، وعدد رينولدز على خصائص انتقال الحرارة، معبراً عنها بتوزيع رقم نوسلت المتوسط على امتداد سطح الارتطام، وتم استخدام حزمة حركيات الموائع الحسابية التجارية "فلونت" لمحاكاة الحالات المختلفة، وتشير النتائج إلى اعتماد انتقال الحرارة بشدة على ارتفاع وعرض القناة، والمسافة بين الفوهة والهدف، وزاوية الدخول، وكذلك على عدد رينولدز.

درجة الماجستير في العلوم

جامعة الملك فهد للبترول والمعادن

الظهران- المملكة العربية السعودية

CHAPTER 1

INTRODUCTION

1.1 Overview

In Feb. 2010, a Cessna 208B (as shown in Fig. 1-1), a domestic scheduled passenger aircraft, sustained substantial damage during impact with terrain following takeoff from Kwigillingok Airport, Alaska, U.S.A. A post accident inspection disclosed no mechanical anomalies with the engine or its accessories, and the airplane was flown to its base after the wing was repaired without any engine problems noted. A weather study by a Safety Board meteorologist determined that the area was subject to light snow showers, freezing fog and mist, and surface temperatures below freezing, all conducive to wing/airframe icing. During an interview with Federal Aviation Administration inspectors, the pilot acknowledged seeing "a trace of ice" on the wings.

Figure 1-1: A Cessna 208B passenger aircraft [1]

In Nov 2010 an ATR-72-212 passenger plane, was destroyed completely in an accident near Guasimal, Sancti Spiritus Province, Cuba, (see Figs. 1-2 and 1-3). All 61 passengers and 7 crew on board were killed. Civil aviation officials concluded that "the flight was proceeding normally until it found itself in extreme meteorological conditions that caused the airplane to ice up severely at an altitude of 20,000ft (6,100m). This, in conjunction with errors by the crew in managing the situation, caused the accident".

Figure 1-2: Wreckage of the ATR-72-212 aircraft in Cuba [2]

Figure 1-3: Registration number of the crashed aircraft [2]

It is now a well established fact that ice formation on critical aircraft surfaces severely degrades the aerodynamic performance of the aircraft. Ice accretion on lifting surfaces (see Fig. 1-4) reduces the lift, increases the drag and weight. This ice accretion results in an increase in the stall speed and a reduction in the stall angle of attack. Therefore, an aerodynamic stall can occur before the stall warning systems can detect it. In propellers, ice drastically affects the efficiency and causes an imbalance resulting in vibrations. In helicopters the rotor blades degrade in their efficiency using more power for equivalent lift causing the aircraft to descend higher than the normal rate. Ice on the canopy reduces the cockpit vision heavily. Communication antennae may be rendered ineffective or even snap off. Extension of flap may result in rudder ineffectiveness or even increase in stall speed. In addition to these problems, the detached ice may also cause unexpected problems such as flame out or compressor stalling when ingested into the jet engine.

Figure 1-4: Icing up of the aircraft lifting surface [3]

Figure 1-5: Severe icing on the wing of an aircraft [3]

Ice accumulates on the leading edges of wings (see Figs. 1-5 and 1-6), tailplanes, and vertical stabilizers as an aircraft flies through a cloud containing super-cooled water droplets. Super-cooled water is water that is below freezing, but still a liquid. Normally, this water would turn to ice at 32°F (0°C), but there are no "contaminants" (ice nucleus) on which the drops can freeze. When the airplane flies through the super-cooled water droplets, the plane becomes the droplet nucleus, allowing the water to freeze on the surface. This process is known as accretion. Droplets of supercooled water often exist in stratiform and cumulus clouds.

Figure 1-6: Icing up of the aircraft surfaces [3]

A popular misconception is that aircraft icing events result from the weight of accreted ice on the airframe. This is not the case. Rather, airframe icing causes problems by modifying the airflow over flight surfaces upon which the ice accretes. When ice accretes on aerodynamic lift surfaces, such as the wing and tailplane, the modification of airflow changes the aerodynamics of the surfaces by modifying both their shape and their surface roughness, typically increasing their drag and decreasing their lift [5]. The particular effect of icing on the aerodynamics of a lift surface is a complicated function of the ice shape and location as well as of the amount of ice [6]. These characteristics in turn depend in a complicated fashion on atmospheric conditions such as the amount, temperature, and droplet size of water in the air [7]. The composite effect of this aerodynamic deterioration over all lift surfaces is a degradation of aircraft flight dynamics. In severe atmospheric conditions, dangerous levels of icing can be obtained in as little as five minutes [8]. Small to moderate amounts of icing generally cause a reduction in aircraft performance in terms of climb rates, range, endurance, and

maximum speed and acceleration. Icing effects of this type are known as performance events. As icing increases, separation of air flow from the flight surfaces can cause loss of pilot control and even wildly unstable behavior. These more severe icing events, known as handling events, are often precipitated by a change in the aircraft configuration or an aircraft maneuver affected by a pilot unaware of the flight-dynamics degradation.

To sum up the topic, the negative effects of Ice buildup are:

1. Destroys smooth flow of air over wing, leading to severe decrease in lift and increase in drag forces.
2. Can change pitching moment.
3. As angle of attack is increased to compensate for decreased lift, more accumulation can occur on lower wing surface.
4. Causes damage to external equipment such as antennae and can clog inlets, and cause impact damage to fuselage and engines
5. Considered a cumulative hazard because as ice builds up on the wing, it increasingly changes the flight characteristics

Icing related accidents have led the U.S Federal Aviation Administration (FAA) to take a renewed interest in aircraft icing related research and a revision of related regulations. FAA In-Flight Aircraft Icing Plan [9, 10] outlined validation and reliability tasks for icing and anti-icing simulation methods being used in the aircraft certification.

A data of most relevant aircraft accidents since 1991 where ice accretion on an aerodynamic surface was the primary or one of the probable causes is shown below in

Table 1-1 It was taken from the National Transportation Safety Board (NTSB) [11] and Flight Safety Foundation's database.

Table 1-1: Business, regional, and transport aircraft icing accidents since 1991

Year	Site	Air Carrier	Aircraft	Phase
1991	U.S.A	Ryan Airlines	McDonnel Doughlas DC-8-63CF	Takeoff
1991	Russia	Aeroflot	Antonov AN-12B	Landing
1991	Russia	Tartarstan Airlines	Antonov AN-24	Landing
1992	U.S.A	USAir	Fokker F-28	Takeoff
1993	Macedonia	Palair Macedonian	Fokker 100	Takeoff
1994	U.S.A	American Eagle	ATR 72-212	Landing
1994	Russia	North Western Air Trasnport	Antonov AN-12B	Landing
1995	Italy	Romanian Banat Air	Antonov AN-24B	Takeoff
1997	U.S.A	Comair Airlines	Embraer EMB120-Brasilia	Landing
1998	Canada	Private	CRJ-200LR	Takeoff
1999	Turkey	Turkish Airlines	Boeing 737-400	Takeoff
2000	Russia	Vologodskiye Airlines	Yakovlev YAK-40	Takeoff
2002	U.K	Private	Bombardier CL-600-2B16	Takeoff
2004	U.S.A	Private	Bombardier CL-600-2A12	Takeoff
2004	China	China Eastern Airlines	Bombardier CRJ-200LR	Takeoff
2005	U.S.A	Private	Cessna Citation 560	Landing
2006	China	China PLA Air Force	KJ-200	Landing
2007	Russia	Private	Bombardier CL-600-2B16	Takeoff
2008	Armenia	Belavia	Bombardier CL-600-2B19	Takeoff

2009	U.S.A	Empire Airlines	ATR-42-320	Landing
2009	Canada	Transwest Air	de Havilland Canada DHC-6 Twin Otter 100	Takeoff
2009	U.S.A	Colgan Air	de Havilland Canada DHC-8-402 Q400	Approach
2009	Russia	Yakutsk Ask Rosto	Antonov 2	Approach
2010	U.S.A	Ameriflight	Beechcraft C99	Landing
2010	U.S.A	Grant Aviation	Cessna 208B Grand Caravan	Enroute
2010	Cuba	Aerocarribean	ATR-72-212	Enroute
2011	Argentina	SOL Lineas Aereas	SAAB 340A	Enroute

From the above table it can be noticed that on an average there are about 1.3 icing related accidents occurring every year. It is seen that the average has increased suddenly to four accidents in 2009 and three in 2010, and a single accident in 2011. All of the accidents were fatal in terms of life. Although a lot of research is being focused on the improvement of hot-air anti-icing systems for aircraft, looking at the trend of accidents, it is interesting to note that still more work needs to be done and new and effective methods need to be developed to enhance effectiveness of anti-icing systems. We cannot fight nature, but certainly find out techniques to control its effect on us.

1.1.1 Types of Ice Accumulation

1.1.1.1 Rime

This type of ice has a rough milky white appearance and generally follows the surface closely as shown in Fig. 1-7.

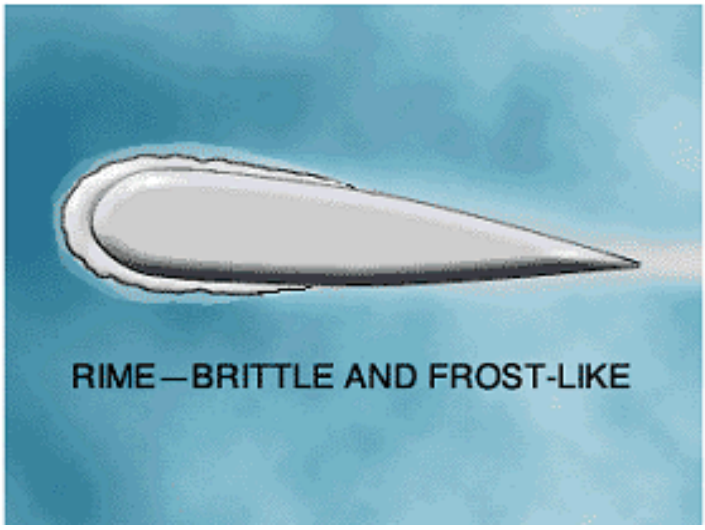

Figure 1-7: Side view of wing with rime [4]

1.1.1.2 Clear

This type of ice is sometimes clear and smooth but usually contains some air pockets that result in a lumpy translucent appearance, denser, harder and more difficult to break than rime ice as shown in Fig. 1-8.

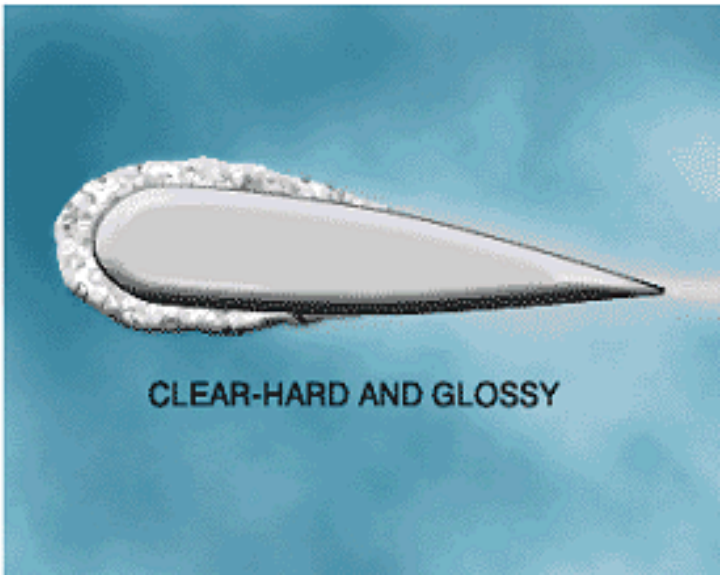

Figure 1-8: Side view of wing with clear ice [4]

1.1.1.3 Mixed

This type of ice formation is a combination of rime and clear type of ice making it the most strong among them all and difficult to break among the three as seen in Fig. 1-9.

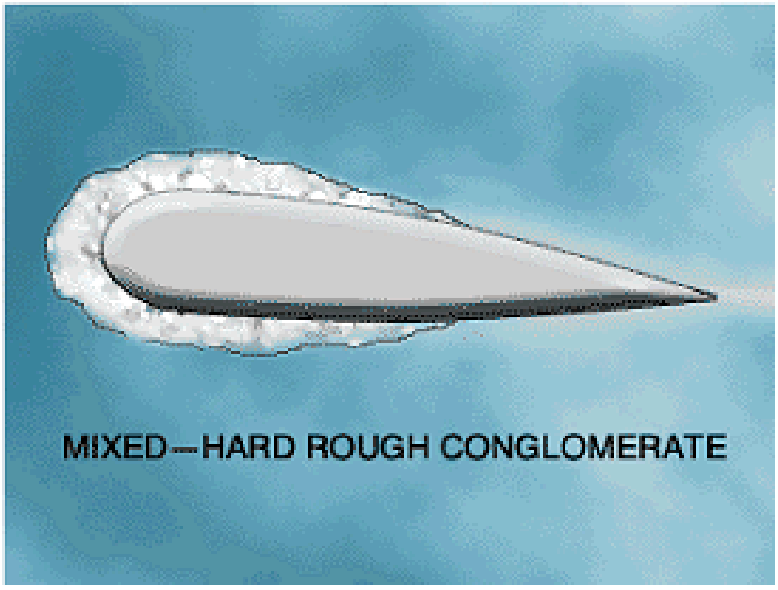

Figure 1-9: Side view of wing with mixed ice [4]

1.1.2 Types of Anti-Icing Systems

In order to avoid the problems pertaining to icing on the aircraft, the aircraft manufacturers typically make use of anti-icing system. Aircraft anti-icing system help prevent ice accumulation on important aircraft surfaces. Although there are de-icing systems also, but they are generally used after the ice is formed so as to remove it by mechanical methods (scraping, pushing); through the application of heat; by use of dry or liquid chemicals designed to lower the freezing point of water (various salts or brines, alcohols, glycols); or by a combination of these different techniques, whereas anti-icing system removes as well as prevents ice-formation, thus performing a dual function. There

are different types of anti-icing systems used today which are designed to prevent ice accumulation. These anti-icing systems include:

1.1.2.1 Electrical Type

Electric heaters are used to heat critical areas. Although it is effective in preventing ice accretion in the leading edges of wings and stabilizers, it requires a large electrical current to be effective over a large area. An example of this is ThermaWing which is manufactured by Kelly Aerospace Thermal Systems.

ThermaWing (Fig. 1-10) uses a flexible, electrically conductive, graphite foil attached to a wing's leading edge. Electric heaters are usually flexible enough to use as anti-icers or de-icers. Once activated an exact concentration of heat melts the bond between ice and protected surface. Ice no longer sticks to the surface due to aerodynamic forces. As an anti-icer, the heater keeps the surface warm so that ice does not form.

Figure 1-10: Thermawing sheet over the airfoil [4]

1.1.2.2 Pneumatic Type

The system is equipped with black rubber boots on the leading edges of wings and

stabilizers in most turboprop and piston aircrafts. The rubber boots inflate and deflate alternatively in cycles flexing the accumulated ice. On failing to deform, the accumulated ice cracks and detaches from the aircraft surface. Under certain conditions, the ice shapes deform and form a bridge over the boots rendering them ineffective.

The pneumatic boot (Fig. 1-11) is a rubber device attached to a wing's leading edge, invented by the Goodrich Corporation (previously known as B.F. Goodrich) in 1923. Portions of the boot are alternately inflated and deflated to break ice off the boot, de-icing the wing. Rubber boots are used on jets and propeller driven aircraft.

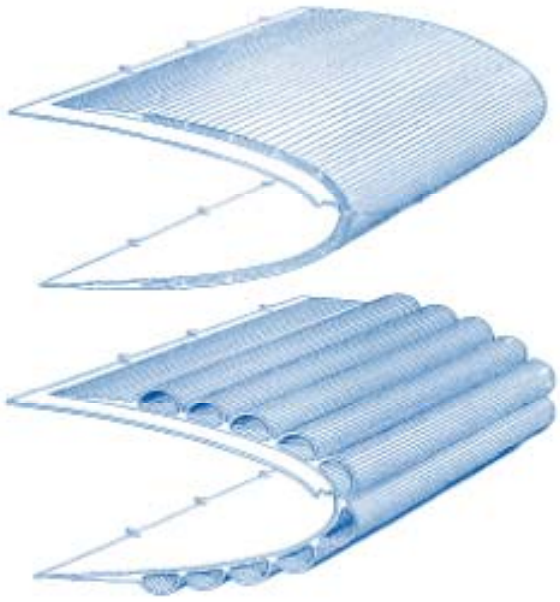

Figure 1-11: Goodrich pneumatic boots inflate to break ice formation on leading edge[3]

1.1.2.3 Hot-Air Jet Type

In many aircrafts, hot-air from the compressor bleed is supplied to the wing's/slat's leading edge through ducts (see Fig. 1-12 (a)). When the hot-air is impinged along the

length of the wing (Fig. 1-12 (b)), it helps eliminate ice by heating the surface. Similarly, areas around the jet intake can be protected from ice formation at the expense of engine power. Some typical anti-icing systems used on 2 of the major aircrafts are discussed below

- Lockheed C-130 Hercules:
  - Engine bleed air used for anti-icing wing and empennage leading edges, radome, and engine inlet air ducts.
  - Electrical heat provides anti-icing for propellers, windshield, and pitot tubes.
- Boeing 777:
  - Engine bleed air used to heat engine cowl inlets. If leak is detected in Anti-Ice duct, affected engine Anti-Ice valves close.
  - Wing Anti-Ice System provides bleed air to three leading edge slats on each wing. Wing Anti-Ice is only available in flight.

It is the most common anti-icing system used today on the aircrafts. It is also the focus of this study and therefore the next section gives some detailed description of a typical hot-air jet anti-icing system

1.1.3 Hot-air Anti-Icing System

A typical aircraft wing system is shown in Fig 1-12. The hot-air anti-icing system uses bleed air from the engine compressor to heat the wing leading edge through the piccolo

tube. This tube has several nozzles along its length maintaining a particular distance. The hot-air is impinged upon the inner surface of the slat or wing's leading edge. As the surface is heated, ice on the outer side melts in the vicinity of the impingement region, thereby also preventing ice accumulation.

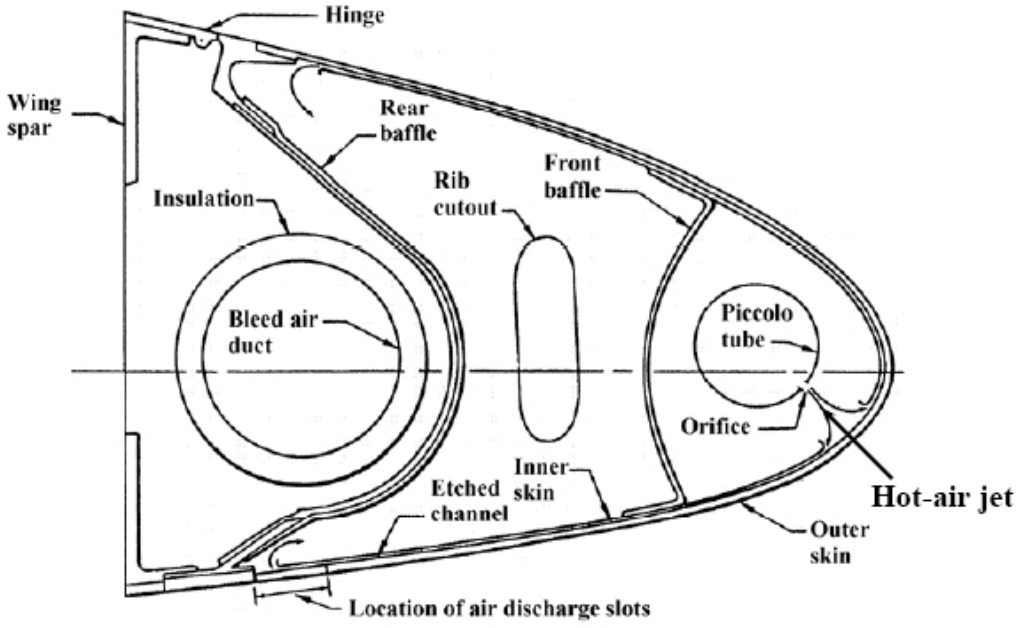

(a) Typical wing leading edge

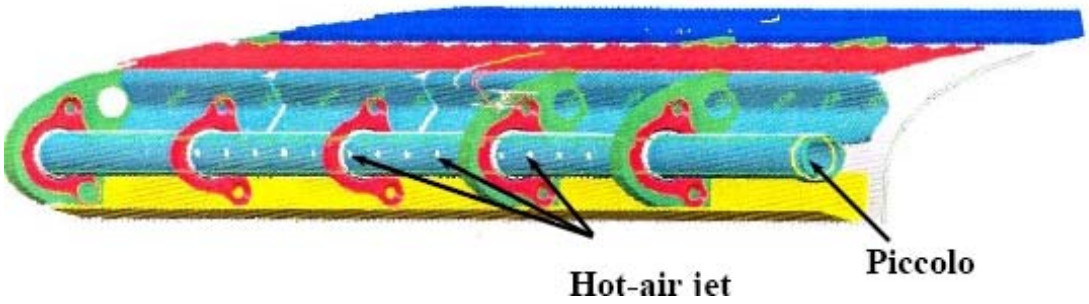

(b) A typical slat

Figure 1-12: Internal layout of the piccolo tube [33]

There are other systems which can be used for anti-icing in an aircraft but all of these have one common drawback that they eliminate ice at the cost of engine performance [12]. In order to minimize the use of engine resources, only a handful of investigators [13-17] have focused their attention on improving the anti-icing system. In addition, only a few studies focused on complex interactions of jet and curved surfaces [14-16] typical of wing leading edge. On the other hand, jet impingement on a flat surface is commonly used in industries in different processes and therefore an extensive literature [16-19] on industrial applications is available today. Most of the literature focuses on key parameters such as jet nozzle-to-surface spacing, jet Reynolds number, jet diameter, jet nozzle-to-nozzle distribution, etc so as to improve the efficiency of the system. A brief overview of the related literature is given in the next section.

1.2 Motivation

It is essential to note that the hot air used for the anti-icing system is taken from the engine compressor bleed and is therefore, a strain on the engine resources. Utilizing this energy in the most efficient way is as necessary as efficient use of fuel for greater economy. A significant amount of heat energy taken from the compressor bleed air for anti-icing system is wasted as a result of inefficient use of the bleed air since the bleed air that exhausts into the atmosphere after being used by anti-icing is still warm. In order to utilize most of the heat energy in the bleed air, it becomes imperative to study the interaction between the hot–air jet and curved surfaces and investigate mechanisms that can aid in enhancing surface heat transfer.

Numerous experimental and numerical studies have been performed to increase the efficiency of the jet impingement based anti-icing system. Most of the investigations

focus on either orifice design [20-23] or the impingement region of target surface geometry. It is an established fact that the surface heat transfer drops off sharply past this impingement region. Although, investigators have studied the use of multiple jets to enhance surface heat transfer over a larger area, use of multiple jets is a further strain on engine resources. The idea of enhancing heat transfer over a larger area using single jet is the focus of this study. Literature review suggests different mechanisms that can aid in enhancing heat transfer over a greater area such as increased turbulence [20-24] or jet intermittency [25].

1.3 Thesis Outline

Chapter one, the introductory chapter, gives an overview of this thesis which deals with improving performance of current aircraft icing systems. The chapter gives a brief introduction to aircraft anti-icing systems and presents an approach to improve the effectiveness of the hot-air jet based aircraft anti-icing system.

Chapter two contains a detailed study of the literature available on jet impingement and different techniques used to enhance surface heat transfer. The research was done irrespective of the field of application. All the support for the investigations was taken from this chapter.

Chapter three illustrates the basic physics and presents the governing equations for the present study including turbulence models available and boundary conditions applied along with material properties.

Chapter four presents the numerical modeling of the various cases developed for simulation in the present study. It also contains details about grid generation and the type of grids used for the study.

All the results are discussed in Chapter five. A classification of results based on parametric variation and heat transfer distribution is presented. Important findings in each result and interesting facts are discussed.

Chapter six outlines the conclusion drawn from this research with recommendations for future study.

CHAPTER 2

LITERATURE REVIEW

Heat transfer enhancement techniques started appearing before 1920, but it was only after 1955 when the number of publications increased tremendously. It was the result of the requirement mainly in chemical, aerospace, power and electronic industries. The second boost in the publications was in 1975 due to the oil embargo, after which about 10% papers in major journals dealt with enhancement. Eventually; by 1991, more than 250 manufacturers offering different products incorporating enhancement technology existed [26]. However, empirical correlations were main part of the experimental investigations. Visual observations gave much new information leading to analytical treatments and numerical studies.

Numerous studies have been carried out to investigate the effects of impinging jet heat transfer with respect to Reynolds number, nozzle-to-plate distance, nozzle geometry, jet temperature, target surface orientation, multiple jets, cross flow, and surface shape on the flow. Many experimented on their idea of different nozzle configuration. Gardon and

Akfirat [27] studied the flow and heat transfer characteristics of two-dimensional and axisymmetric impinging jets with different nozzle configurations. Similarly, Obot et al. [28] investigated the effects of different nozzle geometries on the flow and heat transfer characteristics of round impinging jets.

Popiel and Boguslawski [29] showed how nozzle exit configuration affects the stagnation point heat transfer. Oyakawa et al. [30] measured the heat transfer using three square-edged orifice nozzles with different cross-sections; round, elliptic and cross-shaped.

In 1977, Martin Holgar [18] made an extensive study to derive an empirical correlation for different combinations of arrays of hot jet. He used results of different types of target surfaces heat transfer distribution in terms of Nu distribution. The following empirical correlation gives good agreement with the experiments on single slot jet impinging on a flat surface.

$$\frac{\overline{Nu}}{Pr^{0.42}} = \frac{1.53}{x/2d + h/2d + 1.39}\ \mathrm{Re}^{m(x/2d,h/2d)} \qquad (2.1)$$

$$m = 0.695 - [x/2d + (h/2d)^{1.33} + 3.06]^{-1}$$

Range of validity:

$$3000 \leq \mathrm{Re} \leq 90{,}000$$
$$4 \leq x/d \leq 50$$
$$4 \leq h/d \leq 20$$

The empirical correlation given above is used for validation of numerical predictions in the present research.

In 1993, Zumbrunnen and Aziz [31] used water jet to study the effect of intermittency on convective heat transfer on a constant heat flux surface for both steady and intermittent impinging jets at distances up to seven jet width from the stagnation line (see Fig. 2-1). Their experiments yielded enhancement in heat transfer coefficient of nearly a factor of two, where as theoretical considerations suggested more than this value. They concluded that if the frequency of the intermittency is sufficiently high, the convective heat transfer enhancement increases monotonically.

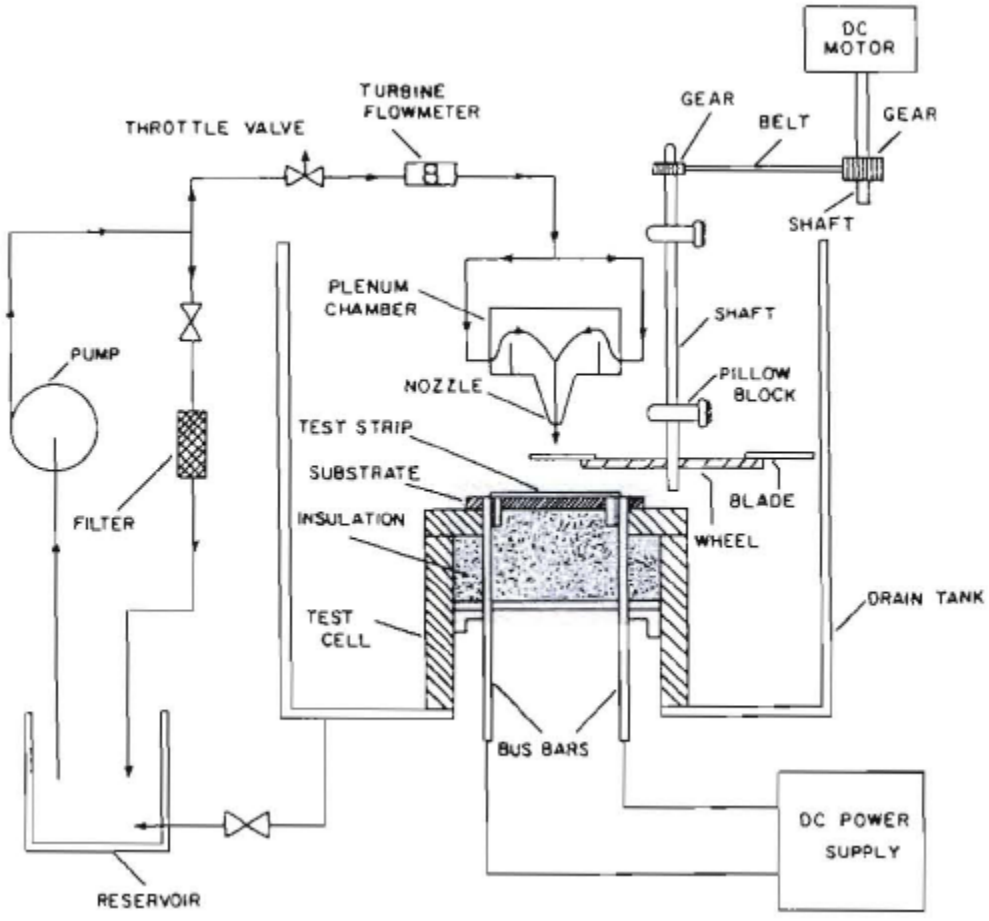

Figure 2-1: Schematic representation of the experimental apparatus of Zumbrunnen and Aziz [31]

A.A. Tawfek [32] in 1996 conducted experiments to determine the heat transfer and surface pressure characteristics of a round jet impinging normal on isothermal plate (see Fig. 2-2). He used three nozzles of exit diameter 3, 5 and 7mm. The Reynolds number used was in the range of 3400 to 41000 and dimensionless separation distance varies from 6 to 58. He found out that local and average heat transfer was a strong function of *r/d* and *z/d*. He found out that heat transfer increases as the jet spacing decreases owing to reduce the impingement surface area. Also the transport rate to the surface increases as jet diameter reduces, where the jet velocity is increased with the same flow rate. He derived a simple correlation of average heat transfer coefficient for all the three nozzle diameters and other pertinent variables.

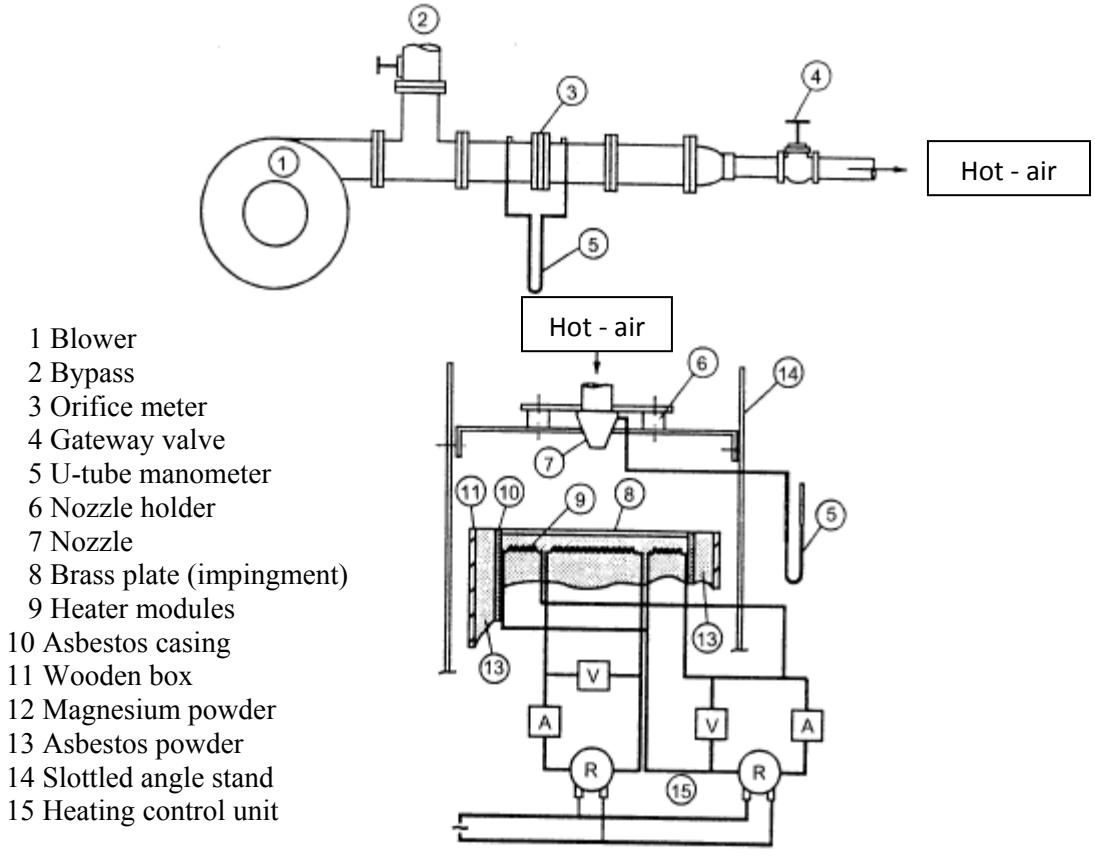

Figure 2-2: Schematic of experimental set-up of Tawfek [32]

$$Nu = 0.453Pr^{1/3}\,(Re)^{0.691}\,(z/d)^{-0.22}\,(r/d)^{-0.38}$$

$$\text{For } 2 \le r/d \le 30,\ 6 \le z/d \le 58 \text{ and } 3400 \le Re \le 41000 \qquad (2.2)$$

Saeed et al. [33] used 2D Navier Stokes CFD code to simulate the jet impingement on a flat plate and modified RAE 2822 airfoil as shown in Fig. 2-3. They used k-ϵ model in CFD code - NSC2KE to validate the numerical predictions. They observed that the present empirical correlations are not reliable enough to use in anti-icing simulations. They developed a new CFD code which can be used for more diversified problems accurately calculating the heat flux, therefore preventing unnecessary loss of energy and resources. Their work developed correlations for both 2D and 3D models [34-35]. Recently, other investigators [36] have also come up with similar correlations.

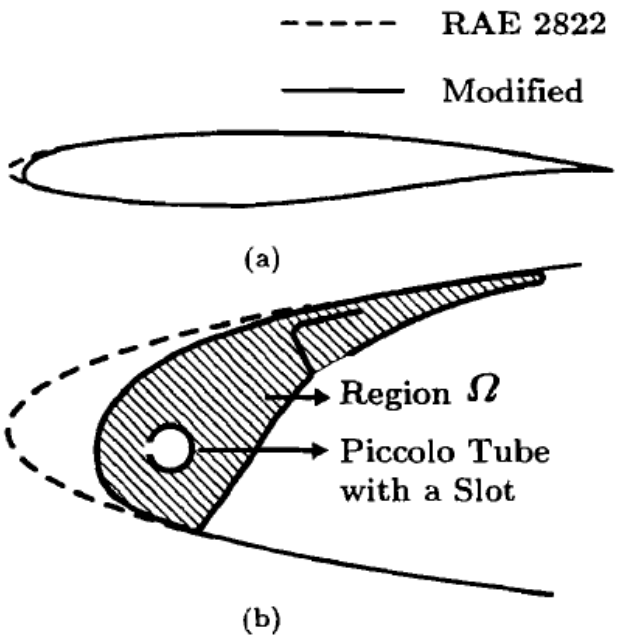

Figure 2-3: The multi-element airfoil used in the study. (a) RAE 2822 airfoil with a modified leading edge to incorporate (b) a typical slat [33]

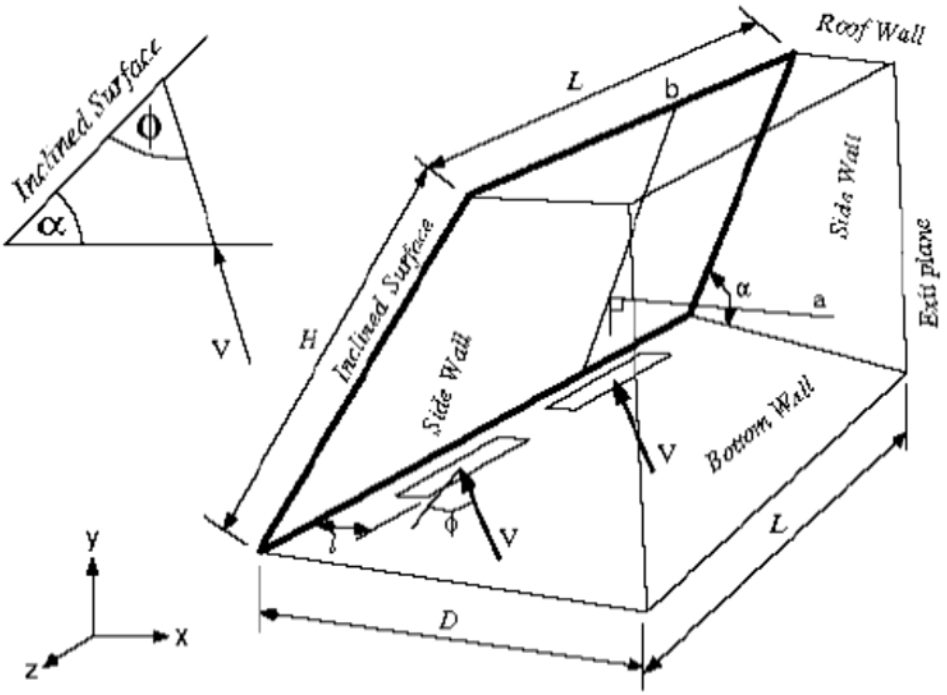

Figure 2-4: Schematic representation of the experimental setup of Patel and Roy [34]

In 2002, Patel and Roy [37] numerically investigated the effect of jet angle and Reynolds number on local and average Nusselt number for a pair of slot jets impinging on an inclined surface as shown in Fig. 2-4. They compared local and average Nu distribution for eight Reynolds number ranging from 500 to 20,000. Also the effect of jet impingement angle on local Nusselt number distribution for a specific line along the solid wall and average Nusselt number for the entire wall were compared for 3 different Reynolds numbers 5000, 10000 and 20000. They found out that average Nu increases as Re increases, i.e. higher flow rates result in higher heat transfer. A correlation between non-dimensional fluid-thermal characteristic parameters was proposed based on the numerical results for a pair of rectangular jets impinging upon a surface. Also a correlation between stagnation Nu, Re, and Pr was proposed. They realized that grid size

is very important especially in high resolution areas like stagnation zone and shear layers for getting better numerical results.

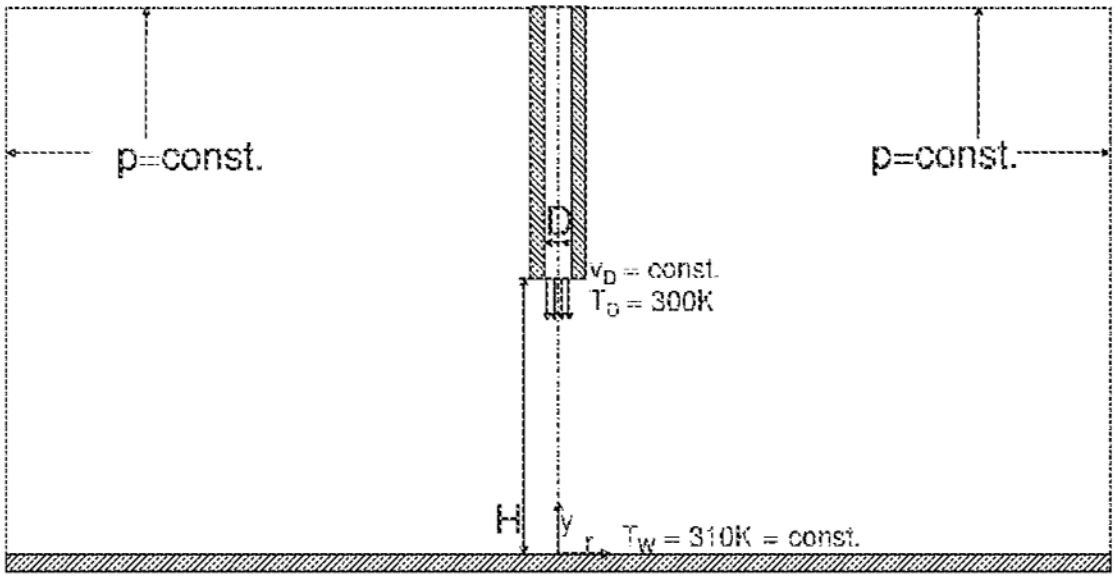

Figure 2-5: Geometry of the model developed by Herbert et.al [38]

In 2004, Herbert et al. [38] used FLUENT version 5.5 to study the results of different turbulence model for jet impingement on hot plate (see Fig. 2-5). They used y^+=0.5 with the grid accommodating 150,000 to 200,000 cells. In that case, the temperature of the wall was a little more than the jet temperature and they used Two-zonal model at the wall. They used the correlation given by Schlunder and Gnielinski [39] to analyze the results. They concluded that the laminar region near the stagnation point cannot be calculated sufficiently well with the turbulence models and increasing the turbulence intensity at the nozzle exit does not improve the results. Hence, heat transfer cannot be calculated sufficiently well with any of the turbulence models in Fluent 5.5.

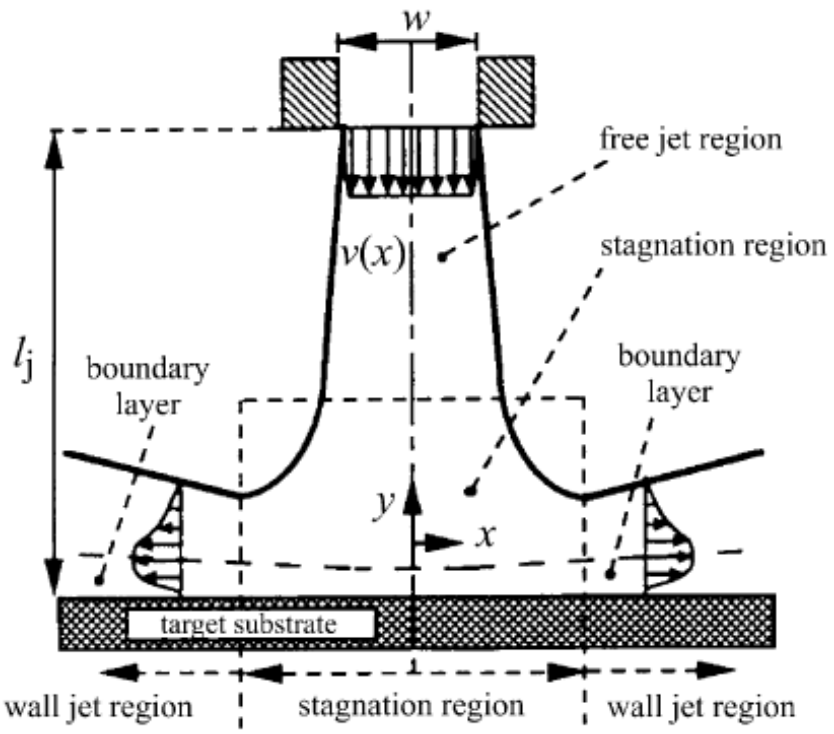

Figure 2-6: Jet Impingement flow region by Sarghini [40]

In 2004, Sarghini [40] did a transient numerical analysis of fluid flow and heat transfer from a planar jet impinging on a finite thickness substrate (see Fig. 2-6). Here a heated target substrate is subjected to a laminar cooling jet with a fully developed profile. He confirmed that the conjugate effect (heat transfer reversal) cannot be neglected during the initial exposition when an opposing cooling jet configuration is realized, for the largest investigated Reynolds number. He concluded that the transient heat transfer distribution showed the presence of heat transfer reversal which has to be considered in processes, as Chemical Vapor Disposition, where it is certainly appreciable and product-sensitive. A similar analysis was done by Shadlesky [41] in 1982.

Papadakis and Wong [21] in 2006 conducted an experimental investigation with a NACA 23012 airfoil in a bleed air laboratory to study the performance of an inner-liner bleed air anti-ice system used in regional and general aviation business jets. Also a computational study was performed on NACA 23012 airfoil and a business jet section. Their intensive investigation was concentrated upon the effect of piccolo design, diffuser geometry and hot-air temperature and mass flow rate on the system performance. All tests were performed using dry cold air flow to cool the exterior of the wing leading edge. The studies conducted showed that after the choking conditions were established further increase in mass flow rate result in small skin temperature gain compared to increase in air temperature, also skin temperatures for the inner-liner bleed air system were sensitive to piccolo placement with respect to the leading edge and to piccolo hole pattern.

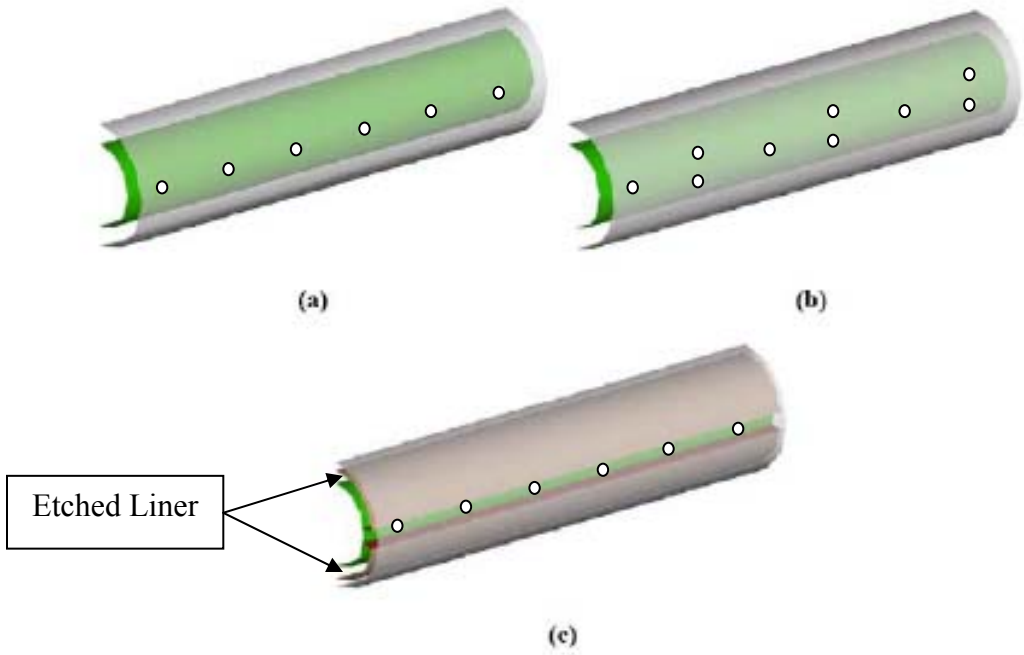

Figure 2-7: The different hot-air jet arrangements used in the numerical study: (a) an array of single jets, (b) an array of staggered jets, and (c) an array of single jets and an etched channel/liner to enhance heat transfer through the outer surface [22]

In 2007, Saeed and Al-Garni [22] conducted a numerical study to simulate heat transfer from an array of jets onto an impingement surface typical of those found on aircraft wing/slats surfaces. Commercial CFD software FLUENT was used for the simulation. They studied the effect of single array of jets shown in Fig. 2-7 (a), two staggered arrays of jets at different stagger angle (10^o and 20^o) shown in Fig. 2-7 (b), and a case with etched surface shown in Fig. 2-7 (c). It was revealed that the single array and the array with a 20^o stagger yield better surface heat transfer than the 10^o stagger. A 2-3 times better surface heat transfer was found in etched surface to others which is a quite helpful observation for future investigations.

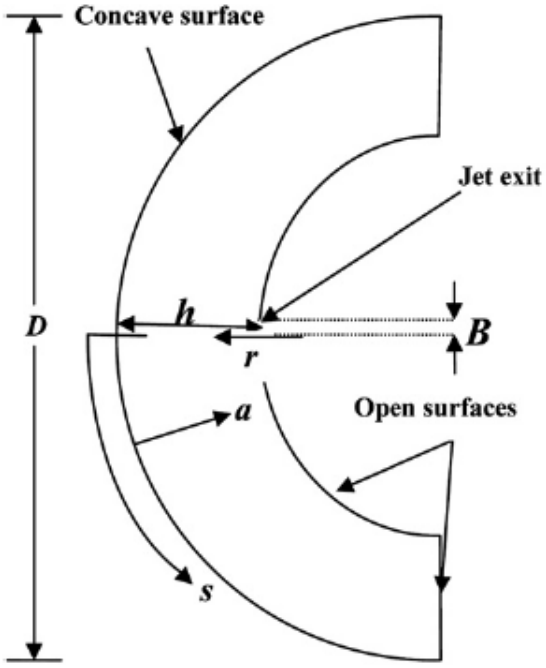

Figure 2-8: Schematic diagram of the slot-jet impingement on a concave cylindrical surface [42]

In 2009, Sharif and Mothe [42] carried out the numerical investigation of convective heat transfer process from concave cylindrical surfaces due to turbulent slot-jet impingement at constant heat flux condition shown in Fig. 2-8. They performed a total of 64 combinations of cases involving changing Reynolds number with jet width *(D/B)* and separation distance *(h/B)*. They concluded that Reynolds number has a significant effect on the heat transfer process. The local Nusselt number at the heated surface increases significantly along any circumferential location with increasing Reynolds number for any set of jet-to-target spacing and relative curvature. The local Nusselt number distribution starts with a high value at the stagnation point with a peak at a slightly offset location from the stagnation point and then and then quickly and monotonically decreases along the heated surface. A correlation for the average Nusselt number as a function of the parameters is derived for the range of parameters considered. They discovered that the heat transfer rate for impingement on curved surfaces was found to increase by an order of 20%.

$$Nu_{avg} = 0.107Re^{0.761}\,(D/B)^{-0.346}\,(h/B)^{-0.047}$$

$$3000 < Re < 12000 \quad 3 < h/B < 12 \text{ and } 30 < D/B < 60 \qquad (2.4)$$

In 2009, Korichi et al. [43] periodically mounted obstacles in a channel with oblique plates as vortex generators as shown in the Fig. 2-9. They modified the direction of the flow towards the obstacle faces to be cooled and activated the self-oscillations using oblique plates placed periodically. Their study focused on analysis of flow evolution and heat transfer enhancement in the intermediate and low Reynolds number range (250-1000) without recourse to turbulent flow. The hydraulic diameter and velocity were

varied from 200 to 2,000 and 0.3 to 5 m/s, respectively. They found that the presence of vortex generators at the upper surface is a powerful mean to enhance the heat transfer compared to basic grooved channel. A 200% increase in heat transfer was obtained for Re = 600.

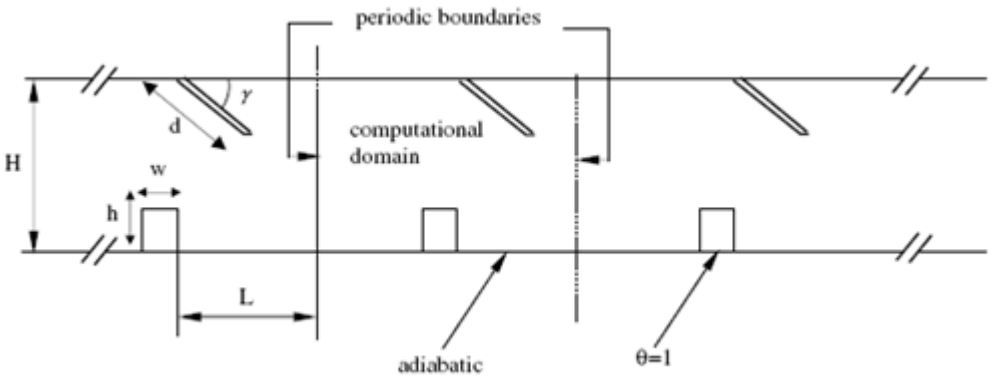

Figure 2-9: Channel with oblique plates and obstacles investigated by Korichi et al. [43]

In 2010, Saeed et al. [44] carried out a numerical investigation of several mechanisms to aid in enhancing heat transfer from an impinging jet typical of those used in aircraft anti-icing system. They investigated five novel internal configurations (see Fig. 2-10) that make use of obstacles to promote turbulence and synergy between flow and heat transfer to enhance heat transfer. These obstacles included a disc, multiple cylinders, a cone, a block facing the hot-air jet impingement surface. The fifth obstacle was a wall liner or etched surface adjacent to the impingement surface. They found out the wall liner technique to be the most promising and effective in enhancing heat transfer through the entire length of the impingement surface. Increase and directed control of turbulence intensity of the other obstacles was also found to be effective but its effect was limited

over a smaller extent of the impingement surface as compared to the wall liner.

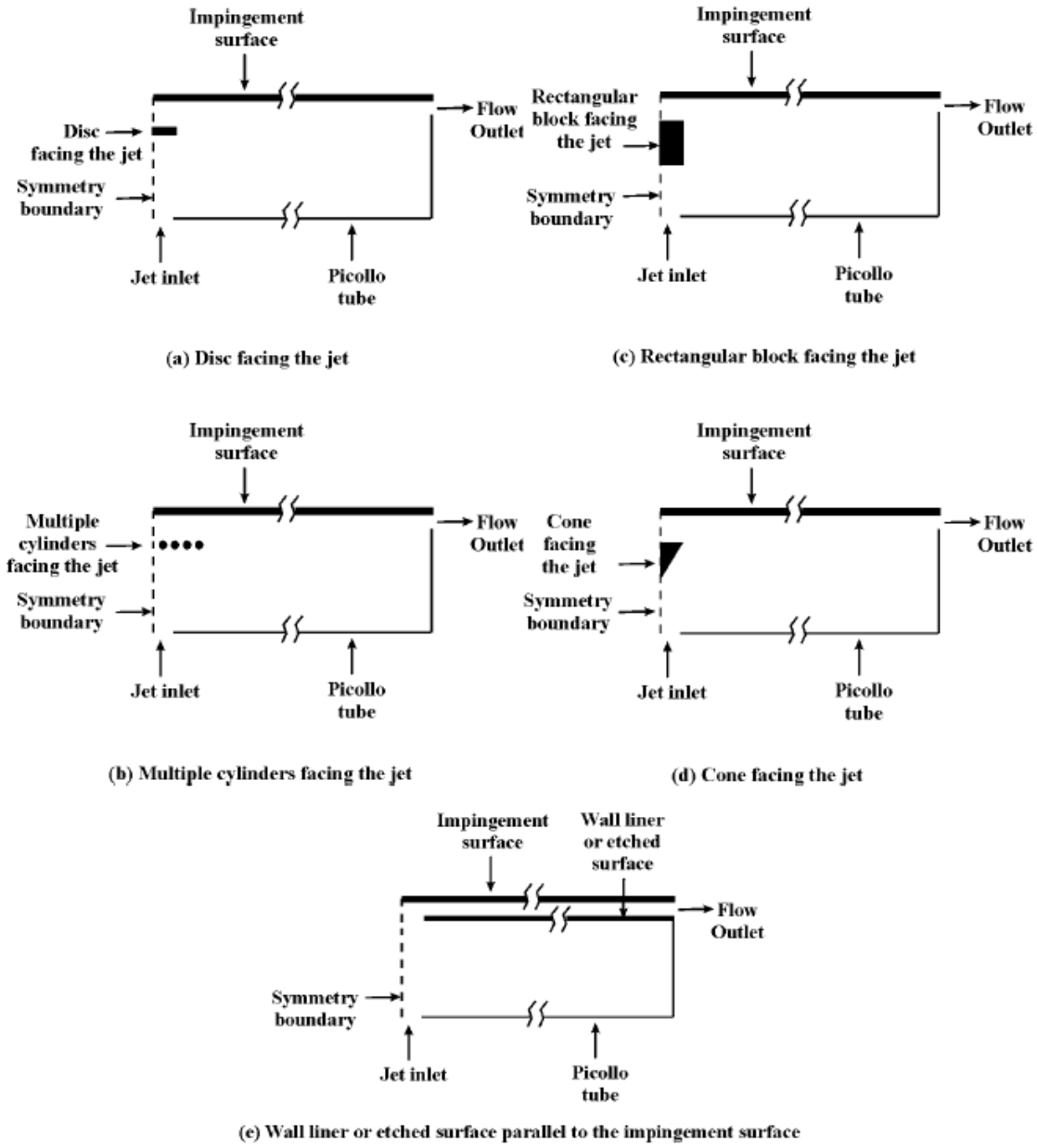

Figure 2-10: Novel ideas investigated in this study [44]

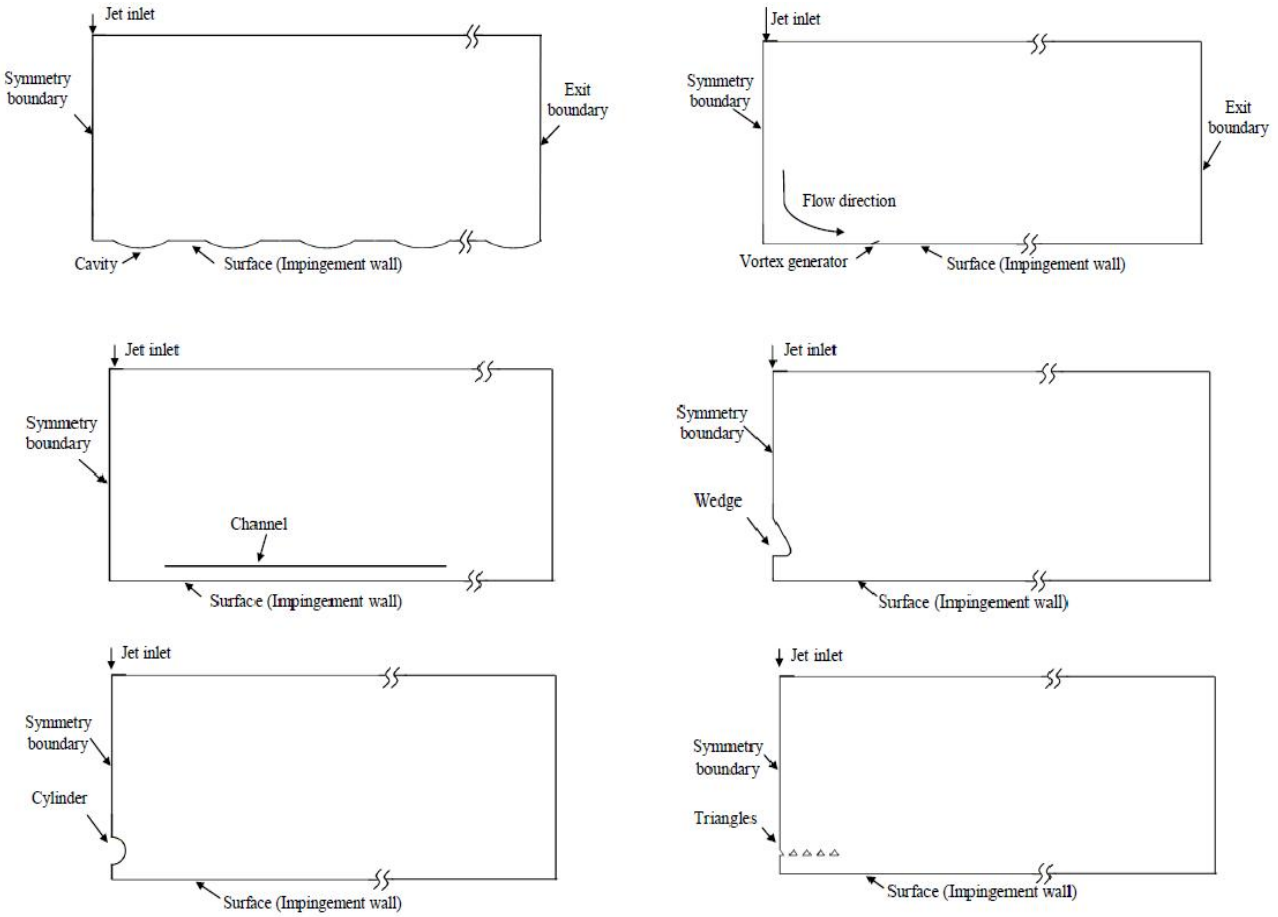

Figure 2-11: Different mechanisms investigated by Ahmed et al. [45]

Ahmed [45] in 2010 studied a number of mechanisms to enhance heat transfer outside the stagnation region (wall-jet region). These mechanisms were a) Jet flow obstructions like triangles, cylinder and wedge. b) Surface liners or restricted channels c) Wall flow or surface obstructions such as vortex generators or cavities (see Fig. 2-11). Of our interest is that he used a free ended channel and numerically investigated it as a surface liner to enhance the heat transfer caused by jet impingement. A trend followed by all the channels was a low heat transfer within the channel and a gradual increase in heat transfer distribution at the exit of the channel. This phenomenon increased overall heat

transfer to a satisfactory level and it was one of the most effective mechanisms for enhancing heat transfer. He suggested further modifications in using a channel to enhance jet impingement heat transfer. The present study is therefore being conducted to answer the question of what is the best channel height for enhancing heat transfer in a hot-air jet anti-icing system.

2.1 Objective of this study

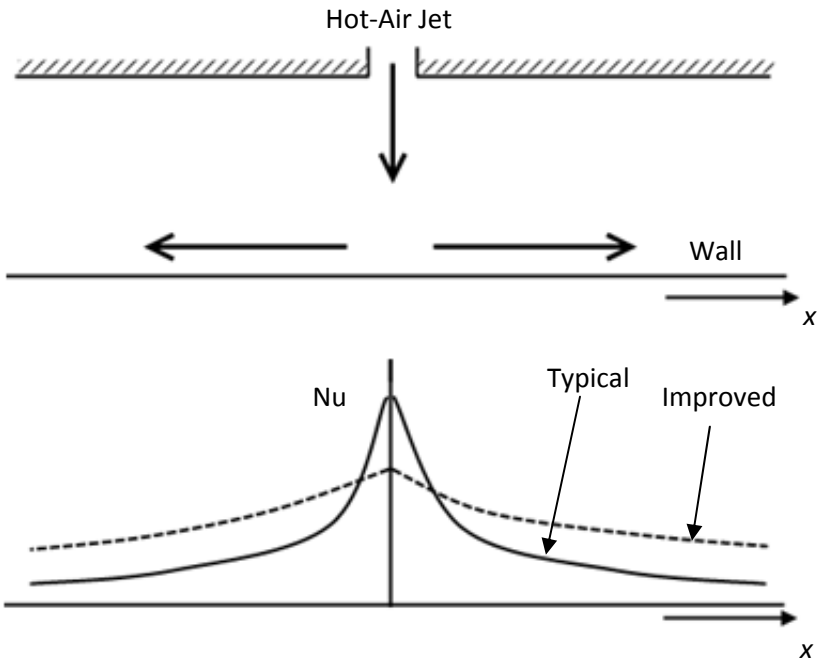

Figure 2-12: Typical and improved surface heat transfer characteristics

Figure 2-12 shows a typical heat transfer distribution from the stagnation point through the wall-jet region along the impingement wall (along x-axis). The heat transfer is represented in terms of Nusselt number Nu along the y-axis. On observing closely, a maximum heat transfer is observed at the stagnation region with a sharp drop-off past the stagnation point. A lower heat transfer is observed therein along the wall-jet region. It

was observed that heat transfer at the stagnation region exceeds the necessary value needed to melt the ice accumulated on the outer side of the impinging wall. Contrary to this, the heat on the wall-jet region was not high enough. Thus, the objective is to achieve improved heat transfer characteristics through a more gradual decrease in heat transfer distribution. Since Saeed [44] & Ahmed [45] have identified liner or channel as the most effective of the mechanisms to achieve enhanced heat transfer in the wall jet region, the focus of the current study is to determine the best placement of the channel.

Thus, this study focuses on numerical modeling and simulation of a channel or an inner liner on the inner side of the leading edge. The objective of the study is to determine the effect of jet distance, channel height, channel location as well as jet Reynolds number on heat transfer characteristics so that the best possible arrangement or configuration could be identified. Moreover, in the current study, a curved impinging surface to simulate a typical wing leading edge is considered as opposed to a flat surface in earlier such investigations [44-45].

The leading edge is simulated using the NACA 23012 airfoil leading edge geometry. Initially a flat plate model is used to validate the numerical model with Martin's [18] empirical correlations, and then the same model with all its dimensions and boundary conditions is transformed into a curved surface model with a NACA 23012 leading edge profile.

2.2 Problem Definition

To accomplish the study, the following objectives were defined:

a. Numerical modeling & simulation of a hot-air jet anti-icing system using channels for enhanced heat transfer.

b. Study and validate a flat plate numerical model with known data in literature. Then develop a numerical model profile with a curved leading edge of a NACA 23012 profile. Validate the model without a channel and establish a baseline model with all the dimensions and boundary conditions.

c. Simulation of a channel or inner wall liner on the inner side of the leading edge.

d. Perform parametric study to investigate the effect of channel height, jet-to-target spacing, channel placement angle, jet Reynolds number on the surface heat transfer.

e. Document and compare the surface heat transfer distribution (average Nu) along the leading edge surface.

f. Report/publish important findings of this study.

g. Make recommendations for future study.

2.3 Methodology

In the numerical simulations, two-dimensional steady flow situation pertinent to a jet impingement inside the wing was considered. The governing equations of flow and heat transfer were solved numerically through employing a control volume approach. Fluent CFD code was used to model the flow of the hot-air region and conduct heat transfer simulations. Fluent solves the Reynolds-averaged Navier-Stokes (RANS) equations which represents the governing equations for fluid flow, using a finite volume method. Turbulent flows were simulated using additional transport equation along with the basic mass, momentum and energy equations. The heat transfer was computed on the wall in the model geometry which is the wing inner surface. Mass flow rate calculated was 0.775 kg/s through the jet inlet at a temperature of 400 K. The viscosity was according to the ideal gas law. The impinging wall was at temperature of 260 K with a thickness of 0.002 m. Thermal conductivity of the aluminum surface was according to the standard value. Validation was conducted using the Spalart Allmaras model and compared to the empirical correlation given by Martin [18].

CHAPTER 3

MATHEMATICAL MODEL

Fluid behavior in the real world follows few basic governing equations. The science of fluid dynamics comprises of these fundamental governing equations - the mass, momentum and energy conservation equations. These equations follow the physics in nature. They are the mathematical forms of fundamental physical principles on which fluid dynamics is based.

3.1 Governing Equations

The governing equations are basically derived from three laws of conservation. They are

1. Conservation of mass (Continuity)
2. Conservation of momentum (Newton's Second Law of Motion)
3. Conservation of energy (The First Law of Thermodynamics)

Velocity V, thermodynamic pressure p and absolute temperature T are the three unknowns found from the solution of the above three conservation equations where

pressure and temperature are considered to be the two required independent thermodynamic variables. Four other thermodynamic variables are present in the final form of conservation equation they are density ρ, enthalpy h, and the two transport properties; viscosity μ and thermal conductivity k .

3.1.1 Conservation of Mass

The conservation of mass law in vector form when applied to a fluid passing through an infinitesimal, fixed control volume yields the following equation of continuity using the Eulerian approach

$$\frac{\partial(\rho)}{\partial t} + \nabla \cdot (\rho V) = 0 \tag{3.1}$$

Rate of density increase + Rate of mass flux = zero

where ρ is the fluid density and V is the fluid velocity

3.1.2 Conservation of Momentum

Newton's Second Law of Motion applied to a fluid passing through an infinitesimal, fixed control volume yields the following momentum equation

$$\frac{\partial\,(\rho V)}{\partial t} + \nabla \cdot \rho VV = \rho f + \nabla \cdot II_{ij} \tag{3.2}$$

Rate of increase of momentum + Rate of momentum lost by convection = Sum of all forces

The stress consists of normal stresses and shearing stresses and are represented by the components of the stress tensor $II_{i,j}$ while f is the force per unit mass.

3.1.3 Conservation of Energy

The First Law of Thermodynamics when applied to a fluid passing through an infinitesimal, fixed control volume yields the following energy equation

$$\frac{\partial E_t}{\partial t} + \nabla \cdot E_t V = \frac{\partial Q}{\partial t} - \nabla \cdot q + \rho f \cdot V + \nabla \cdot (II_{ij} \cdot V) \tag{3.3}$$

where E_t is the total energy per unit volume given by

$$E_t = \rho \left(e + \frac{v^2}{2} + potential\ energy + \cdots\right)$$

q is the energy flux given by

$$q = -k\nabla T \tag{3.4}$$

e is the internal energy per unit mass

$$\nabla \cdot E_t V$$

is the rate of total energy lost by convection through the control surface

$\frac{\partial Q}{\partial t}$ is the rate of heat produced per unit volume by external agencies

$$\nabla \cdot q$$

is the heat lost by conduction through the control surface

3.1.4 Equation of State

In order to relate the thermodynamic properties (μ, k) to thermodynamic variables and to establish relation between the thermodynamic variables (p, ρ, T, e, h) so that the system is closed, the equation of state for ideal gas is utilized

$$p = \rho R T \tag{3.5}$$

where R is the gas constant

3.2 Turbulence Modeling

In a turbulent flow problem, the set of governing equations stated above are insufficient due to fluctuating products including Reynolds stresses and fluxes. Hence, the averaged conservation equations have more unknowns in such situations. This deficiency of governing equations is termed as closure problem. Consequently, there is a need for additional equations to solve the closure problem; turbulence modeling provides additional equations to solve the mean flow equations. These additional equations may be based on empirical observations or physical reasoning and therefore, an ideal turbulence model should introduce the minimum amount of complexity while capturing the essence of the relevant physics.

3.2.1 Turbulence Modeling Equations

Higher values of friction, drag and pressure drop are associated with turbulent flows. Hence, a higher capacity is seen in turbulent boundary layer to negotiate with unfavorable pressure gradients. *Direct numerical simulation* (DNS) method is generally used to solve turbulent flow problems, but it requires resolution of relevant length scales (within the problem domain) including time steps for a steady flow. *Large-eddy simulation* (LES) approach is used for isotropic model and needs large-scale structure of the turbulent flow to be computed directly. Although LES method take almost 1/10th of time than DNS, a time-averaged Navier-Stokes equation is better where stress gradients and heat flux quantities associated with the turbulent motion are dealt in detail. The LES equations are also known as Reynolds equations of motion or the *Reynolds averaged Navier-Stokes*

(RANS) equation. All the conservation equations can be written in the Reynolds average form. Many turbulence models exist in literature today. The choice of the turbulence model depends upon the physics associated with the flow, level of accuracy needed and available time and computational resources.

The turbulence models are classified as

1. Algebraic models
2. One-equation models
3. Two-equation models
4. Stress-transport models

3.2.1.1 Spalart Allmaras Model

The Spalart-Allmaras model [46] solves a single transport equation for a quantity that is a modified form of the turbulent kinematic viscosity. Solving a single equation makes Spalart-Allmaras a simple, fast and reliable turbulence model. Spalart-Allmaras model has been used for aerospace applications involving wall-bounded flows with boundary subjected to adverse pressure gradient.

3.2.1.2 *k-ε* and Realizable *k-ε* model

k-ε turbulence models usually differ in the method of calculating turbulent viscosity, turbulent Prandtl numbers governing the turbulent diffusion of k and ε, and the generation and destruction terms in ε equation. Realizable *k-ε* model satisfies certain mathematical constraints on normal stresses and is consistent with the physics of turbulent flows.

Traditional *k-ε* models poorly solve the dissipation equation, especially in spreading rate for axisymmetric jets where as realizable *k-ε* model uses two new formulae in this aspect. A new eddy-viscosity formula and a new model equation for dissipation ε based on dynamic equation of the mean square vorticity fluctuation. Realizable *k-ε* model has been extensively validated for a wide range of flows, including rotating homogenous shear flows, free flows including jet and mixing layers, channels and boundary layer flows and separated flows.

3.2.1.3 The Shear-Stress Transport (SST) *k-ω* Model

The SST model [47] differs from the standard $k-\omega$ model in two ways, namely; in the gradual change from the standard $k-\omega$ model to a high-Reynolds-number version of the $k-\varepsilon$ model in the outer part of the boundary layer, SST model also has a modified turbulent viscosity formulation to account for the transport effects of the principal turbulent shear stress.

3.3 Boundary Conditions

Boundary conditions play a vital role in defining the domain. They specify the flow and thermal variables on the boundaries of the physical model. The boundary conditions involved in the present domain are shown in Fig. 3-1. A vertical plane along the jet centerline was considered inside the slat as shown in Fig. 3-1 (a). This plane can be stretched straight to form a simple axis symmetric rectangular domain (BB′CC′) as shown in Fig. 3-1 (b) where the OD or OD′ is the line/axis along which the domain is symmetric.

The domain boundary specifications are represented in Table. 3-1 shown below. The piccolo wall is represented by AB and A′B′ with jet slot as AA′. Similarly, the impinging surface is represented by edges CC′ with D or D′ at stagnation point. BC and B′C′ are the outlets for the hot air actually going behind the piccolo tube and finally exiting the system, as seen in Fig. 3-1 (a). It should be noted that in Fig. 3-1 (b), the domain is symmetric along the jet centerline OD or OD′. Also results obtained in such a domain are axi-symmetric. Hence, only the symmetric half region (OABCD) is analyzed to save computational time and resources.

Table 3-1: Domain boundary specifications

Label	Boundary type
OA	Mass Flow Inlet
AB	Wall (Piccolo tube)
BC	Pressure Outlet (Ambient)
CD	Wall (Impinging surface)
OD or OD′	Symmetry (Jet centerline axis)

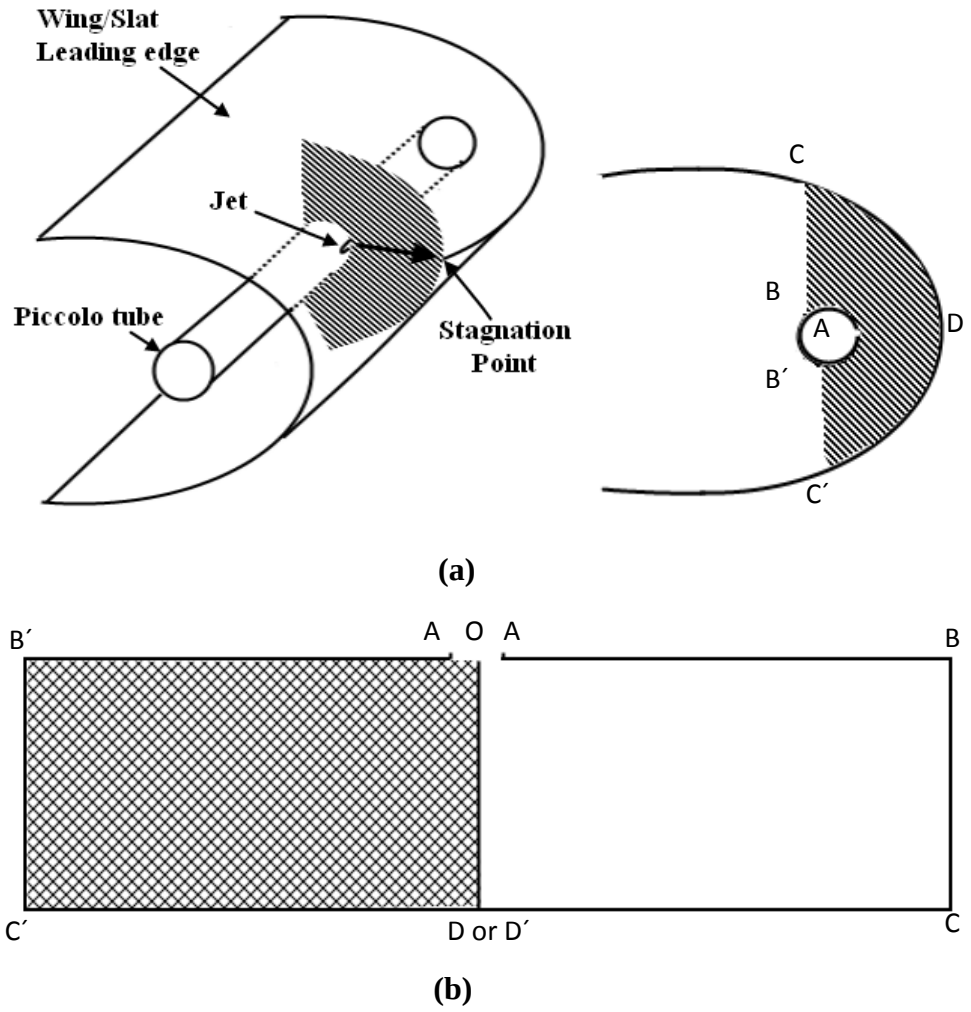

Figure 3-1: (a) Isometric and cross-sectional view of domain location, (c) Domain boundaries

3.3.1 Mass Flow Inlet

The mass flow rate inlet boundary condition is used to model the flow inlet boundary. Air acting as ideal gas is considered to flow out from a jet with Reynolds number 60,000 (V = 34.959 m/s) and viscosity (v = 1.789 × 10^{-5} kg/m-s) at temperature (T_{in} = 400 K).

3.3.2 Pressure Outlet

Pressure outlet boundary condition is used to define the static pressure at flow outlets. An added advantage of this type of outlet boundary condition is that it defines scalar variables in case of back flow. The pressure outlet boundary condition requires the specification of static (gauge) pressure at the outlet boundary. Since the outlet conditions are ambient, zero gauge is defined as the pressure for pressure outlet boundary condition. Ambient pressure is defined as the operating pressure.

3.3.3 Walls and Symmetry

The boundary condition of the impinging wall is a stationary isothermal wall at 260 K temperature exposed to ambient temperature (much lower than the wall temperature) on the other side. The piccolo wall is kept at a constant heat flux with a thickness of 0.002 m.

3.3.4 Numerical Scheme

FLUENT solves the governing integral equations for the conservation of mass, momentum and energy using *segregated* or *coupled* solver. A 2D segregated implicit solver was used as it solves the governing equations sequentially performing solution loop before convergence is reached. First, the fluid properties are obtained and momentum equation was solved. Then the pressure corrections are made by continuity equation considering the current pressure and mass flow rate values. All the other equations including energy, turbulence and scalar equations are then solved and checked for the convergence criteria.

All the cases were modeled in GAMBIT (version 2.4.6) and simulated in 2ddp (two-dimensional double precision solver) in FLUENT (version 6.3.26). The convergence criteria set for all the cases was 10^{-6}. All the cases were simulated on a 2.80 GHz Intel i5 Processor desktop with 4 GB RAM and simultaneously on a 2.10 GHz Intel Core 2 Duo Laptop having a RAM of 3 GB.

Each case took on average about 36 hours to converge. Grid adaption was used to ensure y^+ values were within the limits as suggested in FLUENT manual for the specified turbulence model being used. Each case ran on an average of about 30,000 iterations. Suitable values for post processing were used as given in Table. 3-2.

Table 3-2: Reference values used for post processing

Property (units)	Value
Area (m^2)	1
Density (kg/m^3)	0.887502
Depth (m)	0.025
Enthalpy (j/kg)	102885.3
Length (m)	0.045
Pressure (pascal)	0
Temperature (K)	400
Velocity (m/s)	33.959 m/s
Viscosity (kg/m-s)	1.789×10^{-5}
Ration of specific heat	1.4

3.3.5 Properties

3.3.5.1 Air

Ideal gas law is considered for the fluid (air) at 400 K temperature with viscosity derived from Sutherland's formula given as

$$\mu = \mu_0 \frac{T_0 + C}{T + C} \left(\frac{T}{T_0}\right)^{3/2} \tag{3.6}$$

where μ and μ_o are dynamic viscosity and reference viscosity (μ_o = 18.27×10^{-6} Pa.s), T and T_o are input and reference temperature, and C is Sutherland's constant = 120 K for air.

Specific heat of air is specified in the polynomial form as (in J/kg-K)

$$c_P = 1.045356 \times 10^3 - 3.161783 \times 10^{-1} T + 7.083814 \times 10^{-4} T^2 - 2.705209 \times 10^{-7} T^3 \tag{3.7}$$

Thermal conductivity of air is specified in polynomial form and is given by (in W/m-K)

$$k = -4.937787 \times 10^{-4} + 1.018087 \times 10^{-4} T - 4.627937 \times 10^{-8} T^2 + 1.250603 \times 10^{-11} T^3 \tag{3.8}$$

Which are accurate for 200 ≤ k ≤ 600 K

3.3.5.2 Wall

Properties of aluminum are unitized for the wall material. The isothermal wall (T_{wall}) is at 260 K temperature and has a thickness of 0.002 m.

CHAPTER 4

NUMERICAL MODEL DEVELOPMENT

4.1 Grid generation

Grid generation is often considered as the most important and time consuming part of CFD simulation. It is a process of subdividing the region to be modeled into a set of small control volumes. The quality of grid plays a direct role on the quality of the solution. The solution will be more consistent and efficient when using a well constructed mesh. In the present study, both structured and hybrid grids were used in modeling.

4.1.1 The flat-plate model

From the Fig. 1-12 (b), the domain boundaries were estimated and their dimensions were modeled as shown in Fig. 4-1.

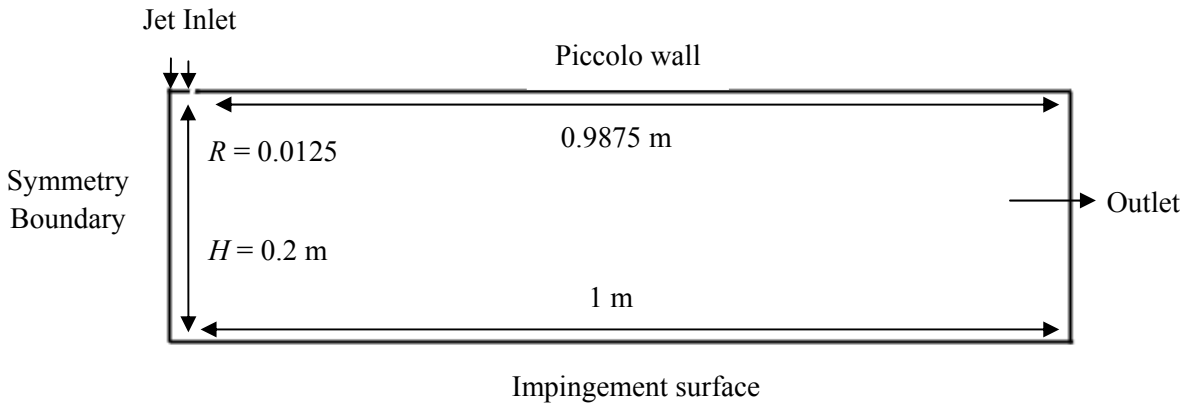

Figure 4-1: The computational domain for jet impingement on a flat surface

4.1.2 Structured Grid

Structured grid allows high degree of control as the user is free to place control points and edges to position the mesh. Structured mesh flow solver typically require low memory to execute the solution faster as they are optimized for structured layout of the grid. In the present study, modeling for the validation and study cases was conducted using a well structured grid within the rectangular domain as shown in the Fig. 4-2. The grid is compressed in one or more coordinate direction to properly resolve the various flow gradients near the walls.

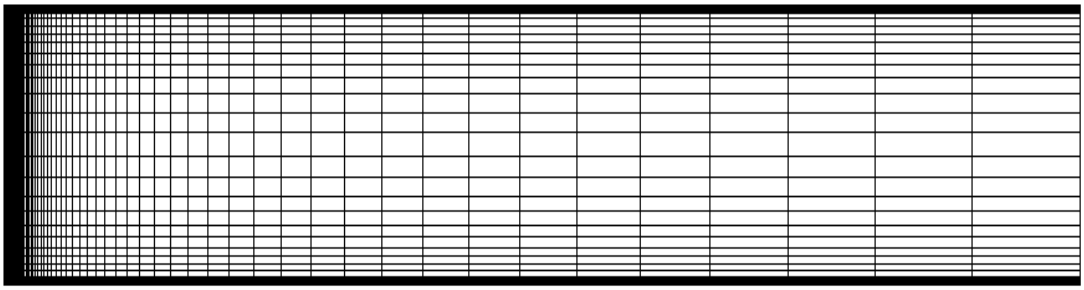

Figure 4-2: Domain discretized using a structured grid

In the present case, the velocity profile near the walls has to be resolved; therefore, the grid is stretched away from or compressed near the walls. A higher velocity and pressure gradient can also be seen near the stagnation point and at the jet boundaries. The grid is thus concentrated towards the jet centerline. It can be easily assumed that the flow along the wall becomes more parallel to it as it moves farther away from the stagnation point. Keeping this in mind, the grid concentration at the right end of the domain is made coarse so as to save computational time and unnecessary calculations.

4.1.3 Hybrid Grid

A structured grid is more economical way of modeling and computationally solving a problem. However, there are many cases in which the geometry becomes complex and intricate where a structured grid becomes very difficult to construct. In such cases, the user is forced to use unstructured mesh to resolve all the regions of the domain. Unstructured grid uses an arbitrary collection of elements to fill the domain. Because the wedge arrangement is not a repeated pattern as in structured grid, the mesh is called unstructured. An advantage of such a grid is that it requires a very little input from the user and are numerically generated using different unstructured grid generation schemes. Thus, the user has very little control over the elements and their arrangement. Hence, this type of grid generation is used when users encounter complex geometry which cannot be meshed using a structural pattern. A geometry may require unstructured grid generation but not in the entire domain. In such cases, a combination of structured and unstructured grid is used where only few faces in the modeling are subjected to the required type of grid. Such a combination of grid is called a hybrid grid.

4.2 The curved-wall model

The flat plate model is transformed into a curved model with similar dimensions and is later validated along with the flat plate model with the empirical correlation of Martin [18]. The curved model resembles that of a NACA 23012 leading edge and is shown in Fig. 4-3.

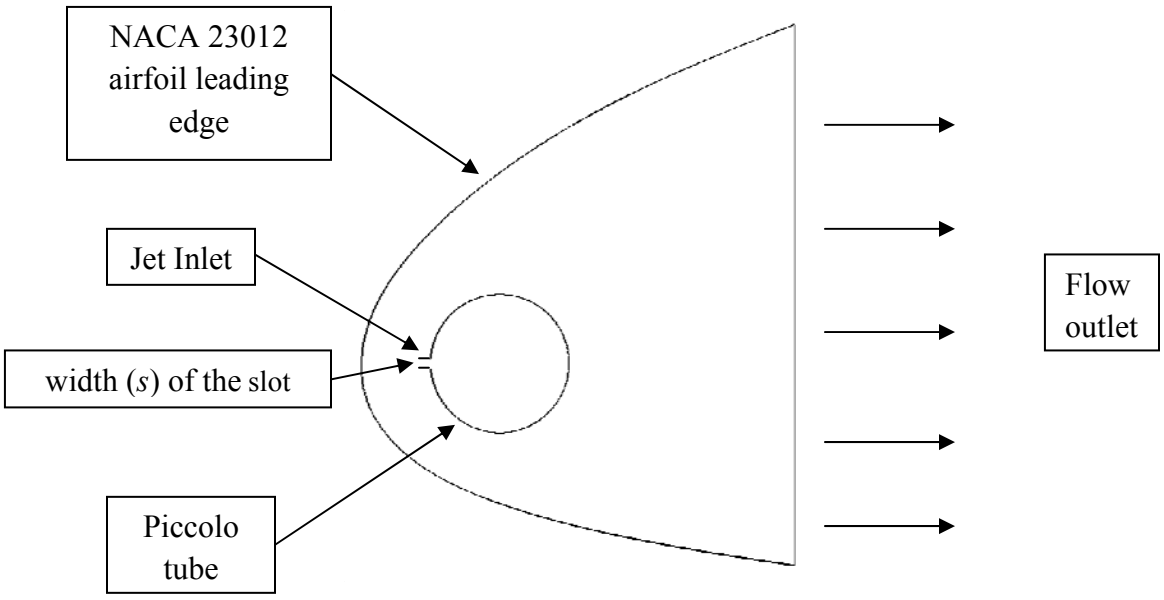

Figure 4-3: Curved-wall model

4.2.1 Curved-wall model grid

The curved model is meshed carefully in order to explore heat transfer at the crucial regions i.e. near the inlet, the outlet, the impinging wall. The meshing used in this model involves a combination of structured and hybrid meshes, with structured near the inlet, outlet and impinging wall and hybrid meshes in the rest part as shown in Figs. 4-4 and 4-5.

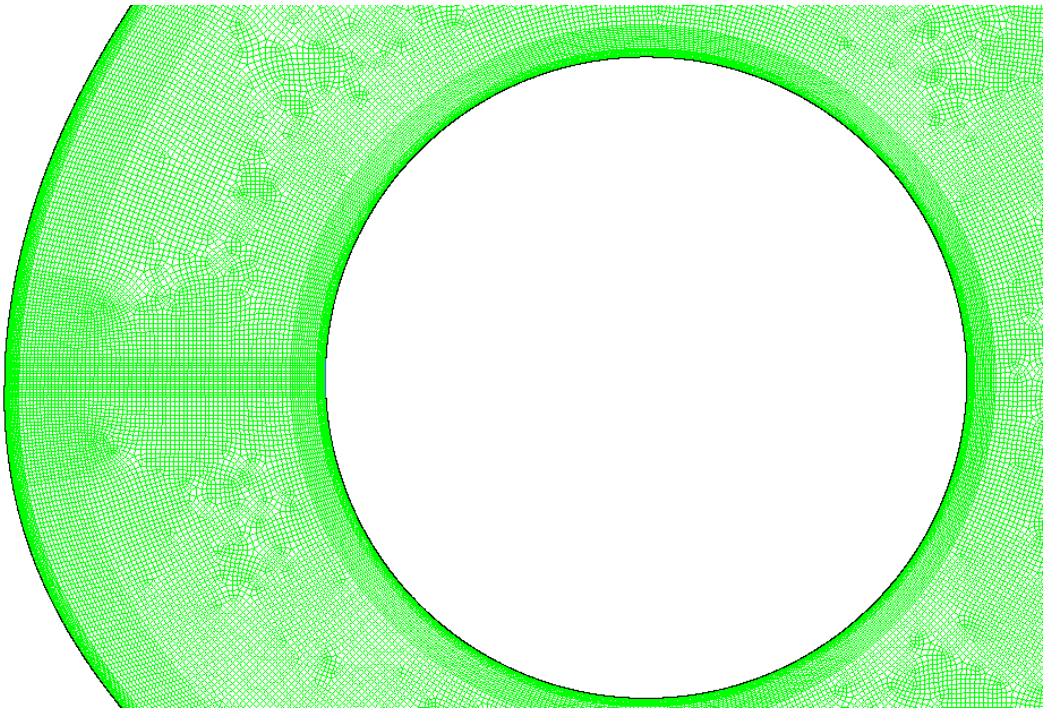

Figure 4-4: Curved-wall model mesh showing piccolo tube

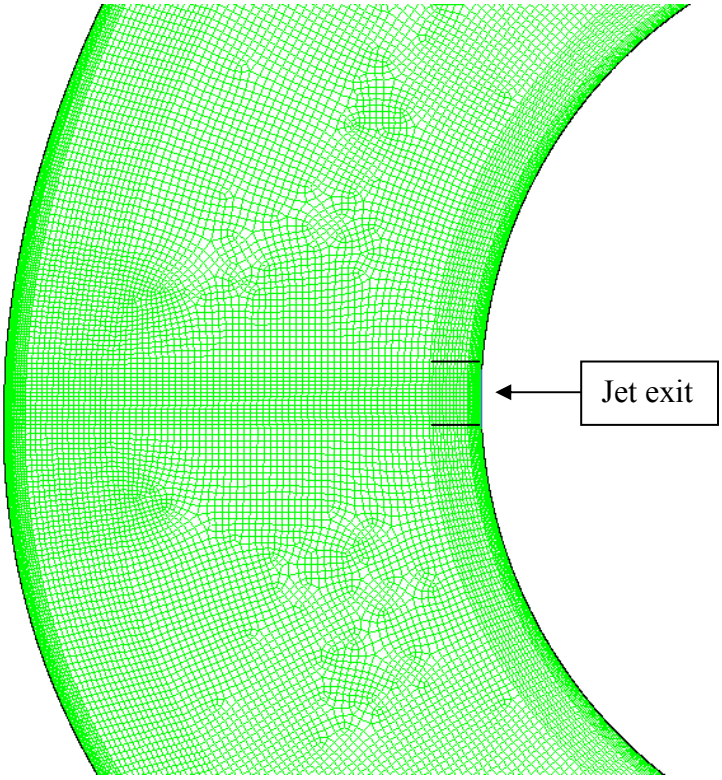

Figure 4-5: Close-up view of the mesh

4.3 Validation

The flat plate model which is shown in section 4.1.1 is validated with the following empirical correlation for surface heat transfer in terms of average Nusselt number given by Martin [18]:

$$\frac{\overline{Nu}}{Pr^{0.42}} = \frac{1.53}{\mathrm{x/2d+\ h/2d+1.39}}\ \mathrm{Re}^{m(x/2d,h/2d)} \tag{4.2}$$

$$m = 0.695 - [x/2d + (h/2d)^{1.33} + \ 3.06]^{-1}$$

Range of validity:

$$3000 \leq \mathrm{Re} \leq 90{,}000$$
$$4 \leq x/d \leq 50$$
$$4 \leq h/d \leq 20$$

Thus for validation study, a slot width of d = 0.05 m, a slot height of H = 0.2 m was chosen. The average flow velocity was chosen to give a jet Re = 60,000 well within the range of Martin's correlation.

Since the results obtained from the numerical solution are in the form of local Nusselt number, they are integrated in order to compare and validate them with the Martin's empirical data in terms of average Nusselt number. The numerical integration is performed using trapezoidal rule which is an approximate technique for calculating the definite integral. If we represent the integration as definite integral

$$\int_a^b f(x)dx$$

where it is assumed that f(x) is continuous on $[a,b]$, we can divide $[a,b]$ into n subintervals of equal spacing:

$$\Delta x = \frac{b-a}{n} \tag{4.3}$$

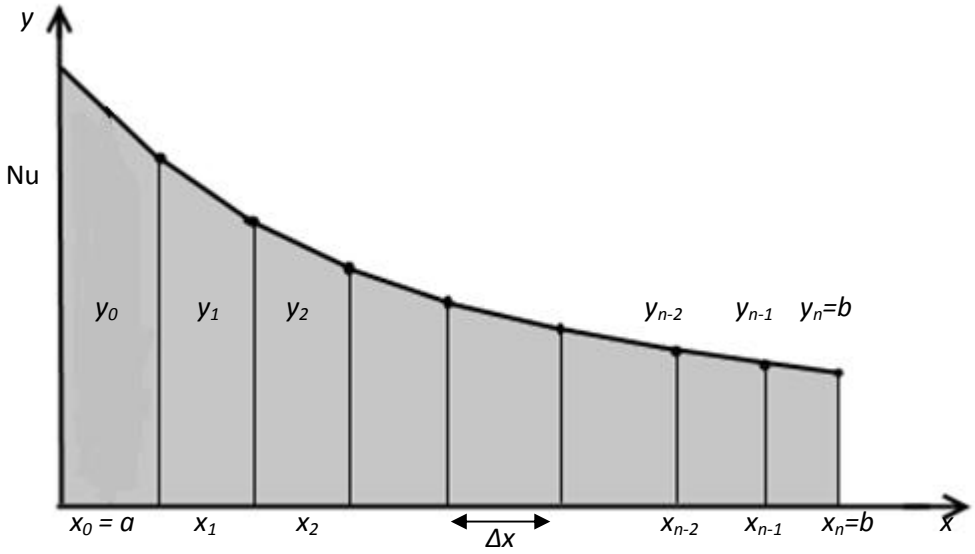

Figure 4-6: Approximating the graph of y = f(x) with line segments across successive intervals to obtain the Trapezoidal rule

Summing the definite integrals over each subinterval provides us with the approximation

$$\int_a^b f(x)dx \approx \left(\frac{y_0+y_1}{2}\right)\Delta x + \left(\frac{y_1+y_2}{2}\right)\Delta x + \cdots + \left(\frac{y_{n-1}+y_n}{2}\right)\Delta x \tag{4.4}$$

which simplifies to the trapezoidal rule formula

$$\int_a^b f(x)dx \approx \frac{\Delta x}{2}\,(y_0 + 2y_1 + 2y_2 + \cdots + 2y_{n-1} + y_n) \tag{4.5}$$

By definition the average Nusselt number is related to the local Nusselt number by the relation:

$$\bar{N}u_{avg}(x) = \frac{1}{x} \int_0^x Nu_{local}\ (x')dx' \tag{4.6}$$

Therefore, the use of trapezoidal rule to calculate the Nu_{avg} leads to the expression

$$\bar{N}u_{avg}\ (x) = \frac{\Delta x}{2}\ [\ Nu_{local}(x_0) + \ 2\ Nu_{local}(x_0 + \ \Delta x) + \cdots 2Nu_{local}(x_n - \Delta x) + \ Nu_{local}\ (x_n)] \tag{4.7}$$

In this thesis, the local Nu number data has been converted to average Nu number data for ease of comparison with the empirical data of Martin [18].

4.4 Parametric Studies – Models & Cases

4.4.1 Effect of jet-to-target spacing

The main motive of this study is to find the optimum channel height and the optimum angle at which the channel should be placed to get the maximum heat transfer. In order to achieve that a series of parametric studies needed to be performed, one of which includes studying the effect of variation of the placement of the piccolo tube which means in the other words the jet-to-target spacing denoted by *z* and is referred to as a non-dimensional parameter *z/d* in this thesis, where *d* is the diameter of the jet inlet.

4.4.1.1 Placement of piccolo tube

According to the literature survey and the initial model development and simulation, the piccolo tube is placed at *z/d* = 8. The model is shown below in Fig. 4-7.

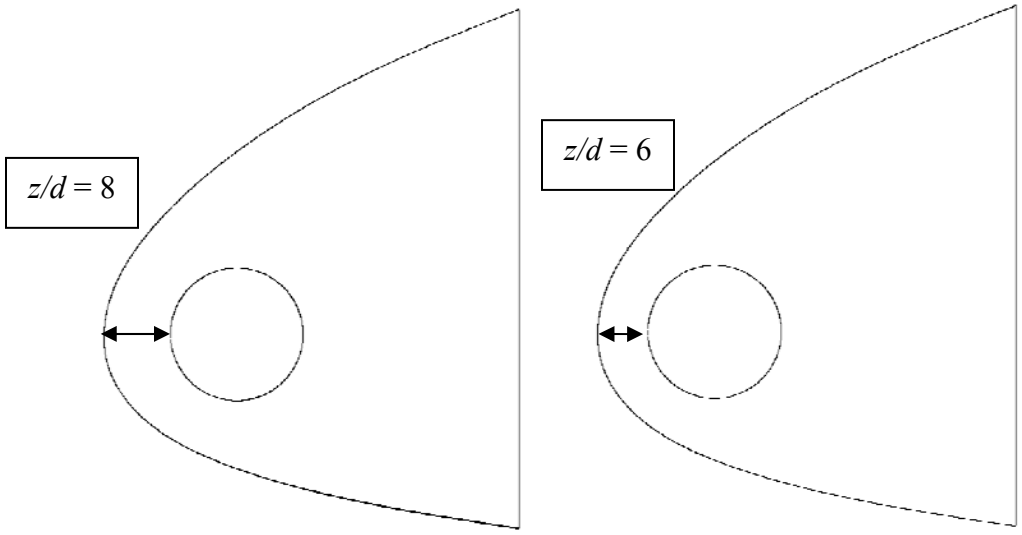

Figure 4-7: Piccolo tube placed at *z/d* = 8 and 6 (right)

The piccolo tube is then moved closer to the leading edge with *z/d* = 6. This is done to find out the optimum heat transfer which will be obtained on either of the one *z/d* used. The piccolo tube is further moved to *z/d* = 4 at which the heat transfer is studied. The model is shown below in Fig. 4-8.

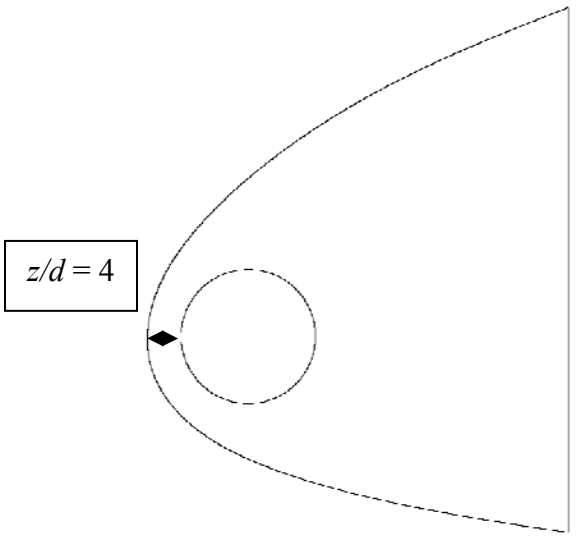

Figure 4-8: Piccolo tube placed at *z/d* = 4

4.4.2 Effect of channel height

After the curved model is formed and validated, five channels are placed inside the curved model near the leading edge at an angle of 10° from the center of the piccolo tube as shown in Fig 4-9. The channels are placed to investigate the effect of their placement on the heat transfer. The channel height is denoted by *h* and is referred to as non-dimensional parameter *h/d* where *d* is the diameter of the jet inlet. The material used for the channel wall is aluminum and is meshed accordingly in order to study the effects of flow near the channel wall (see Fig. 4-10). Care was taken to keep the channel inlet placement angle fixed at 10° when the jet-to-target spacing was varied.

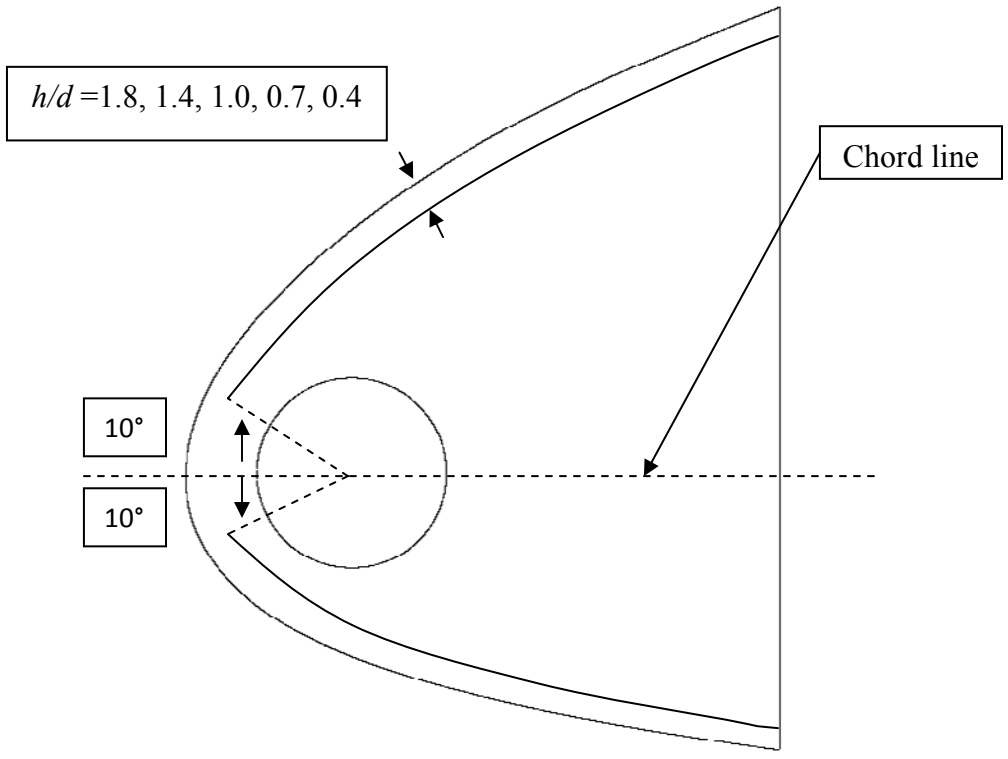

Figure 4-9: The different channel height-to-diameter cases that were investigated

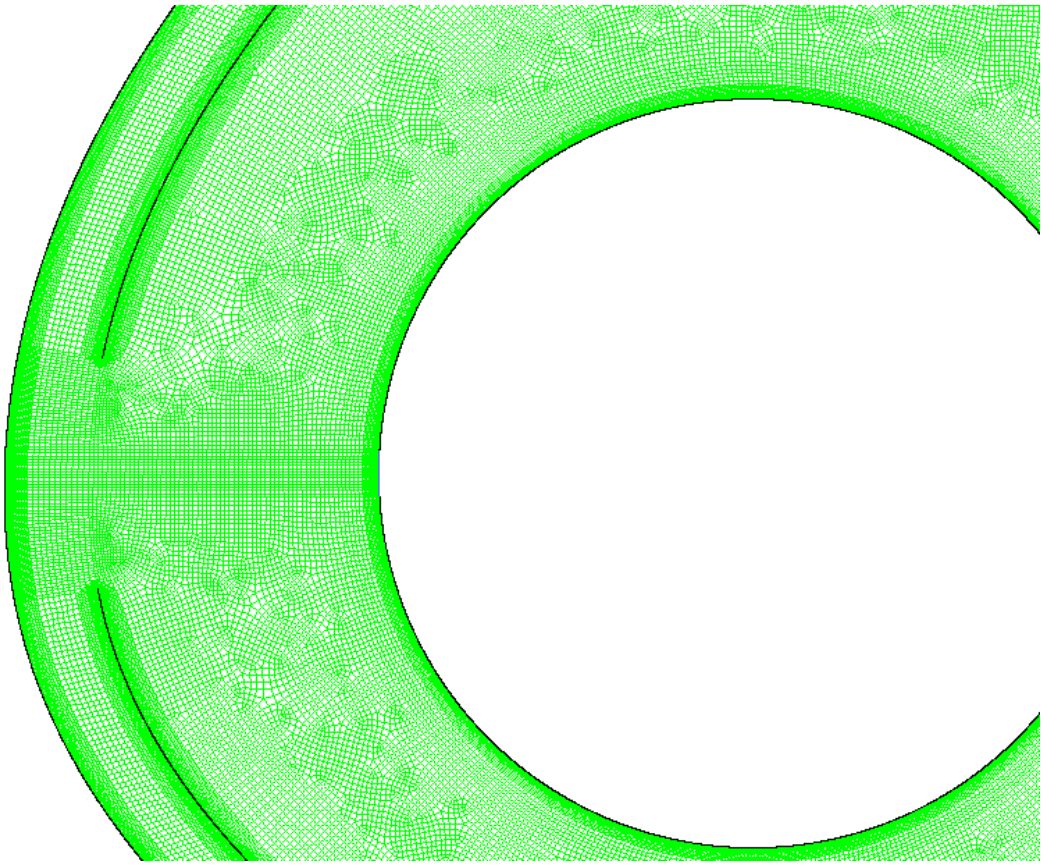

Figure 4-10: Meshing of the channel placed inside the curved model

4.4.3 Effect of Jet Reynolds Number

The Jet Reynolds Number is varied from the initial 60,000 to 30,000 and then to 90,000 to investigate the effect of Reynolds number on heat transfer. The jet-to-target spacing *z/d* is maintained at 6 and cases involving five different channel heights inside the curved model are investigated to determine which channel gives the maximum heat transfer. The jet Reynolds numbers is varied by varying the mass flow rate at the inlet which in turn changes the velocity which gives us the desired Reynolds number. For Re = 60,000 the mass flow rate is 0.775 kg/s, for Re = 30,000 the mass flow rate is 0.385 kg/s and for Re

= 90,000 the mass flow rate is 1.155 kg/s.

4.4.4 Effect of channel inlet location angle

After the variation of the jet Reynolds number the angle θ at which the channel is placed with respect to the center (Fig. 4-11) of the piccolo tube is varied and investigated to find out at which angle the maximum heat transfer occurs. Initially 10° angle is investigated and then the channel is placed at 20°, 40°, and 60° with respect to the piccolo tube center. The channel is placed at these angles with care to place it uniformly on both the upper and lower sides.

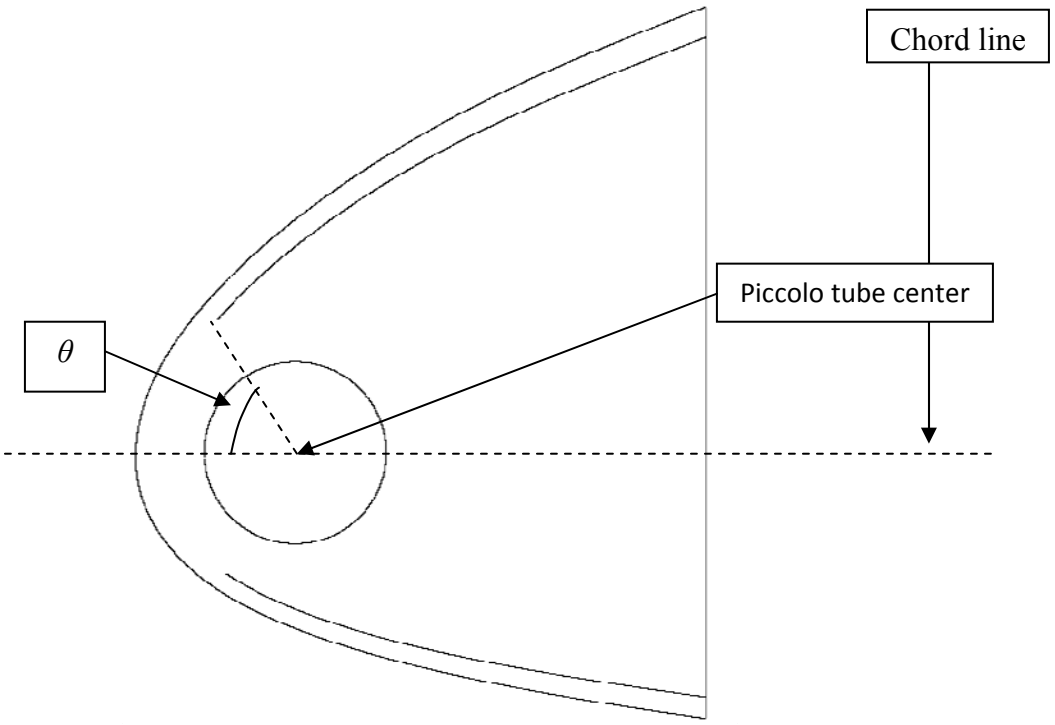

Figure 4-11: The channel inlet location angle θ

In summary, Table 4-1 lists the details of the different numerical simulation cases investigated in this study.

Table 4-1: Detailed configurations of the numerical simulation cases investigated in this study

Case ID #	θ	Re	z/d	h/d					
				A	**B**	**C**	**D**	**E**	**F**
1	10°	60,000	8	0.4	0.7	1.0	1.4	1.8	No Channel
2	10°	60,000	6	0.4	0.7	1.0	1.4	1.8	No Channel
3	10°	60,000	4	0.4	0.7	1.0	1.4	1.8	No Channel
4	10°	30,000	6	0.4	0.7	1.0	1.4	1.8	No Channel
5	10°	90,000	6	0.4	0.7	1.0	1.4	1.8	No Channel
6	20°	60,000	6	0.4	0.7	1.0	1.4	1.8	-
7	40°	60,000	6	0.4	0.7	1.0	1.4	1.8	-
8	60°	60,000	6	0.4	0.7	1.0	1.4	1.8	-

CHAPTER 5

RESULTS & DISCUSSION

5.1 Validation of numerical model

Figure 5-1 compares the Nu_{avg} distribution over a flat surface and a curved surface with the empirical correlation for a flat surface as given by Martin [18]. The empirical correlation was based on experimental data which had a ± 15% scatter. The comparison shows that the flat surface numerical model prediction is within the ± 15% spread in the experimental data for the same jet characteristics (Re*, z/d, T*) as well as wall boundary conditions (T_{wall}, T_{in}). It starts at a lower value because heat transfer increases just after the stagnation region which is around *x/s* = 1 to 2. Moreover the curved surface results show a 10% (approximately) increase, which is due to the fact that heat transfer rate for impingement on curved surfaces increases by an order of 20% which has been reported by Sharif and Mothe [42] as well. The curvature is seen to impart more momentum to the wall jet which results in an increase heat transfer. Lastly the result of the curved model with a channel placed inside it is plotted which is run with the same conditions to

establish a baseline. The results show a significant increase in heat transfer up to 20% compared to the curved model and significantly more compared to the flat plate model. For the channel case, again increase heat transfer can be attributed to increased wall jet momentum close to the inlet to the channel. The greater stagnation point heat transfer can be attributed to the fact that the stagnation region has increased confinement and circulation due to curvature.

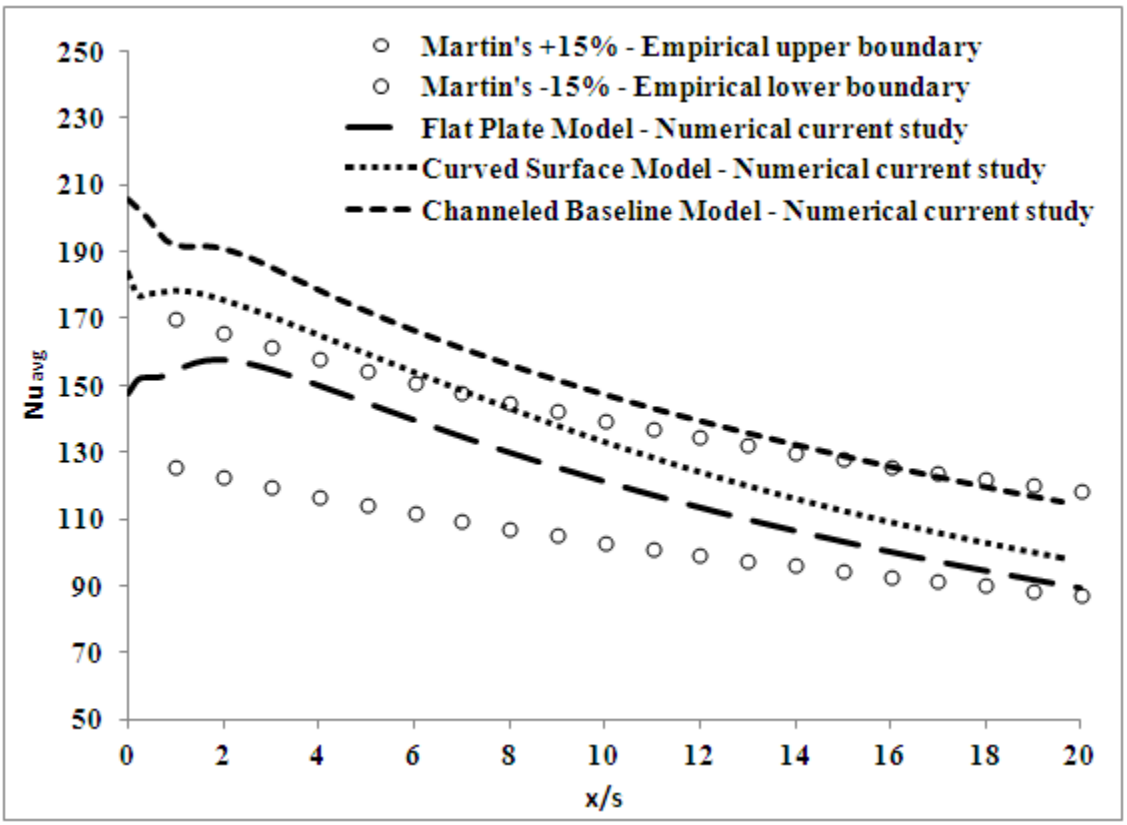

Figure 5-1: Comparison of different numerical models with empirical data

5.2 Effect of jet-to-target spacing

The effect of jet-to-target spacing on Nu_{avg} was studied for z/d = 8, 6, and 4 values. For

each case, five different channel heights were simulated. A case without channel was also simulated for comparison.

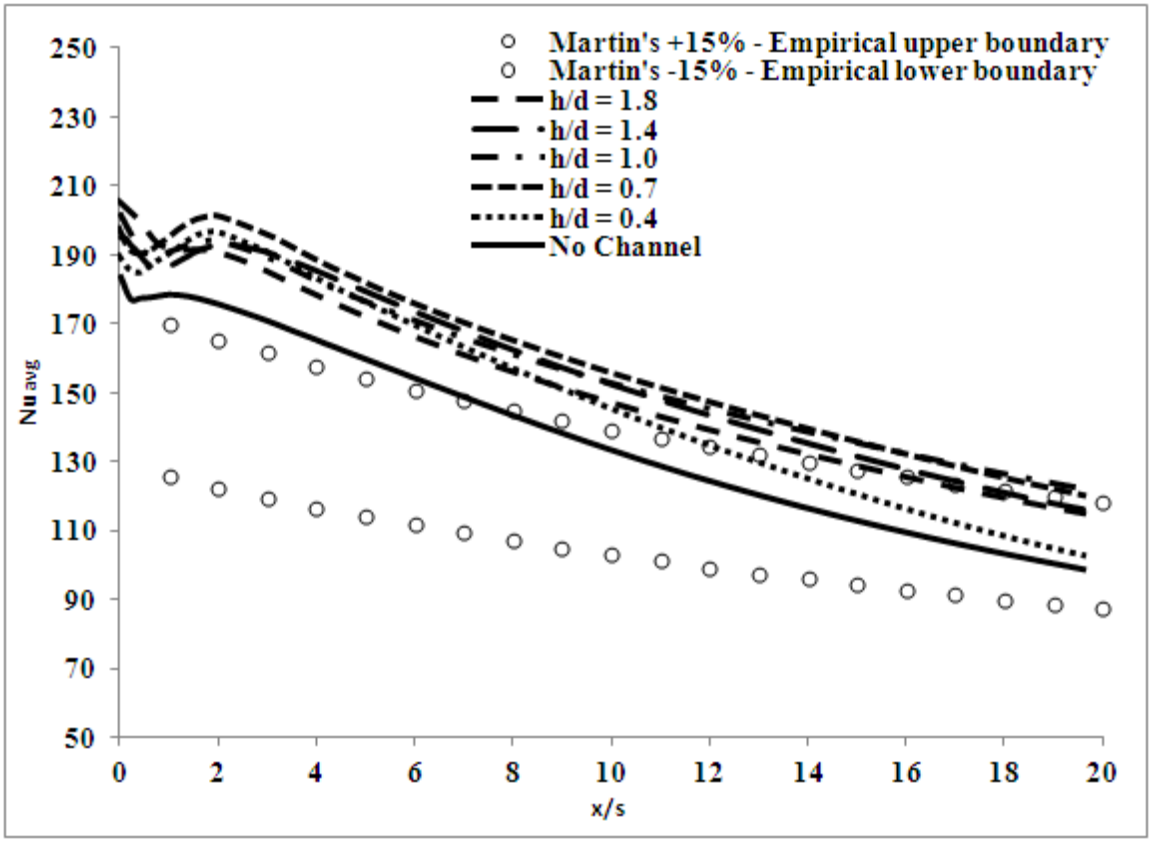

Figure 5-2: Results at *z/d* = 8 with five channels

Figure 5-2 shows the results for the 5 channels placed at a height *h/d* = 1.8, 1.4, 1.0, 0.7, and 0.4 respectively. The jet-to-target spacing of *z/d* = 8 is used in this simulation. The results show all the channels exhibiting somewhat similar heat transfer results. On observation the heat transfer for the channel at *h/d* = 0.4 falls off sharply compared to the other channels after *x/s* = 12. This is due to the curvature shape of the channel around the far wall jet region. The channel placed at *h/d* = 0.7 gives marginally better heat transfer. However it is difficult to conclude with certainty without considering the numerical

accuracy of the results. The overall heat transfer of the channels is high compared to the baseline model. This is due to the fact that a channel is placed which restricts the flow to the impinging wall. The trend followed by all the channels shows a peak around $x/s = 2$ and then gradual fall off. This is due to the presence of channel inlet at that location which is seen to impact more momentum to the wall jet region. This is observed via increase in turbulence and shear stress along the impinging wall. The validity of this reasoning is also confirmed by the fact that the peak does not appear in the case without a channel.

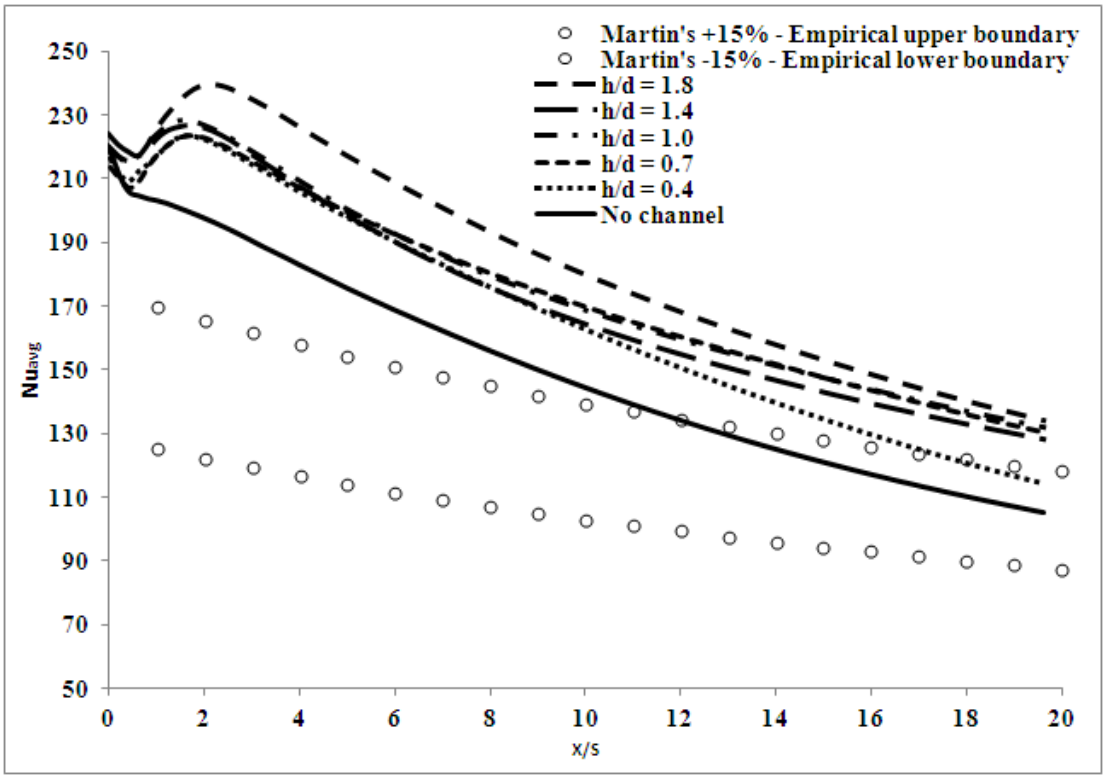

Figure 5-3: Results for $z/d = 6$ with five channels

Figure 5-3 shows the results for various channel heights at $z/d = 6$. The overall heat transfer distribution for $z/d = 6$ is found to be higher than $z/d = 8$. The channel at $h/d =$

1.8 gives slightly better heat transfer compared to the others suggesting the need for investigating additional cases with $h/d > 1.8$ to determine the optimum channel height. One important trend seen is that the heat transfer increases just past the stagnation region and then starts to fall-off gradually. The peak which is occurring at just around $x/s = 2$ is again due to the placement of the inlet of the channel at around that point. The $z/d = 6$ model gives higher heat transfer than the baseline model at $z/d = 8$ indicating that the optimum jet-to-target spacing is around $z/d = 6$.

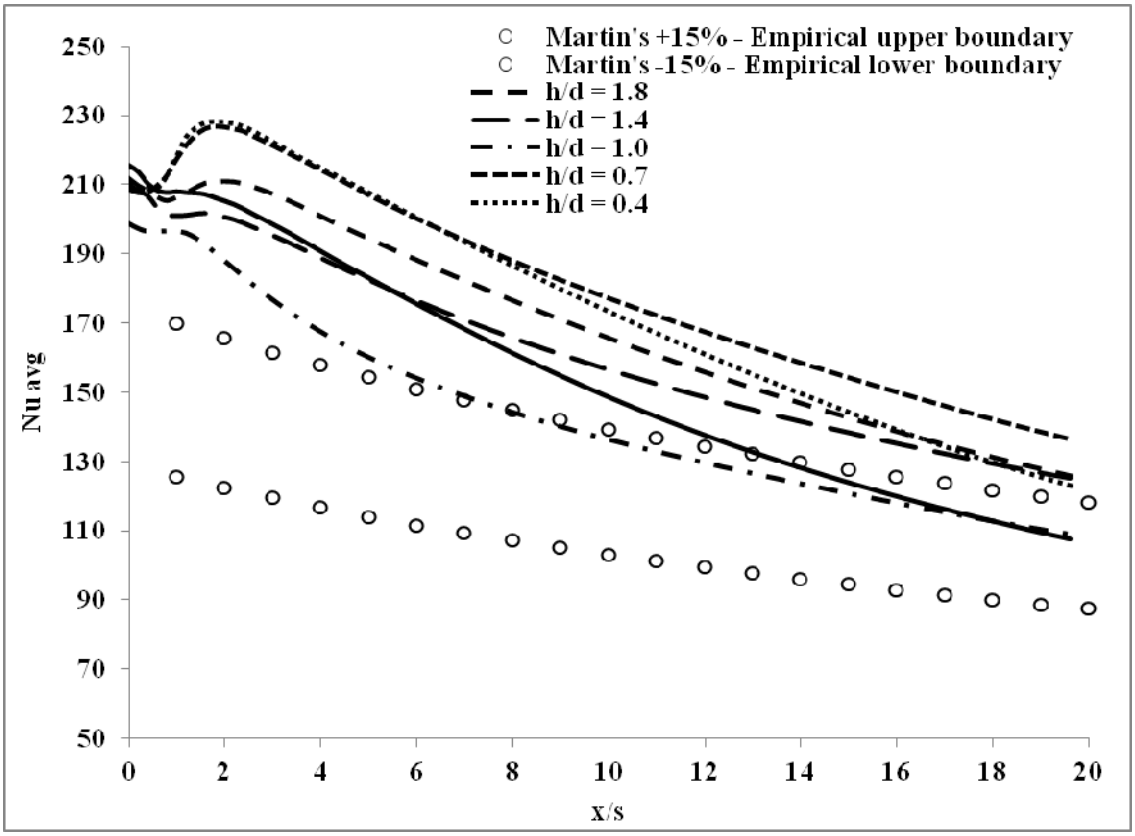

Figure 5-4: Results for $z/d = 4$ for five different channels heights

Figure 5-4 shows the results for different channel heights at $z/d = 4$. The channel at $h/d = 0.7$ gives marginally higher heat transfer than the rest of the channels. Again this is not

very conclusive without certainty of numerical accuracy. The channel placed at h/d = 1.0 gives lower heat transfer compared to the baseline model indicating that this height is not suitable at all. As seen in Fig. 5-5, a trend is observed that as the jet-to-target spacing z/d is reduced from 8 to 4, heat transfer increases from 8 to 6, and then decreases from 6 to 4 suggesting that the spacing of z/d = 6 is closer to the optimum jet-to-target spacing. Livingood and Hyrcak [48] conducted a vast literature survey of experimental and numerical studies on heat transfer due to jet impingement on **flat surfaces** and found that the optimum jet-to-target spacing for a single circular jet should be around 6 – 7 and for a single slot jet should be 8. The present study which involves curved surfaces suggests that the optimum jet-to-target spacing for increasing heat transfer is lower. Furthermore, it also depends on the presence of a channel and the channel height.

5.3 Study of various jet-to-target spacing at fixed channel height

Figure 5-5 presents the heat transfer distributions for a fixed channel height of h/d = 0.4 for various jet-to-target spacing. It illustrates the behavior of each channel at various jet-to-target spacing. The channel at z/d = 6 starts off with a marginally higher Nusselt number value at the stagnation region but the value of channel at z/d = 4 becomes higher at around x/s = 2.

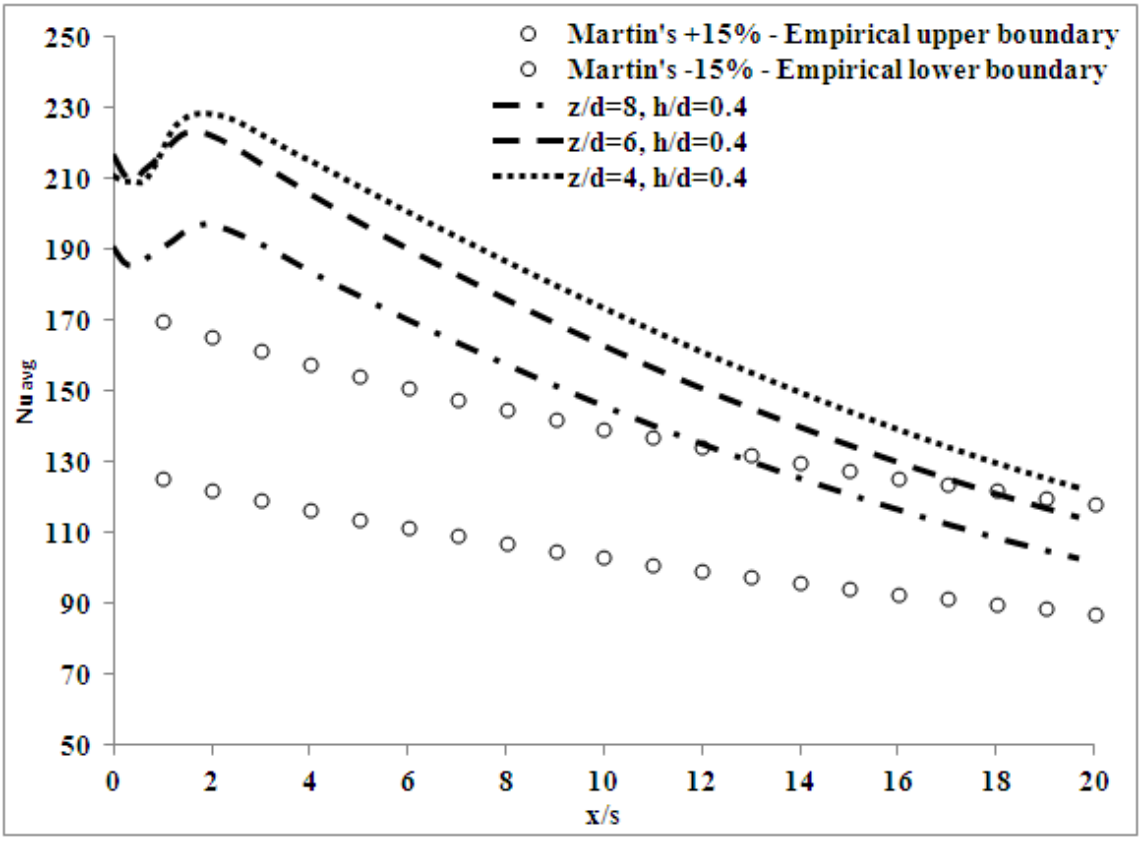

Figure 5-5: Results for *h/d* = 0.4 for different *z/d* = 4, 6 & 8

Figure 5-6 shows the results of various jet-to-target spacing for a fixed channel height of 0.7. All the channels exhibit a similar trend including a peak in Nu_{avg} at around *x/s* = 2 before starting to drop off gradually in the wall jet region. This peak is due to the channel inlet placement which is around *x/s* = 1 to 2. As mentioned earlier, the peak in Nu_{avg} is observed in the vicinity of the inlet to the channel. After this region the flow stabilizes and continues to move down the wall jet region resulting in gradual drop of heat transfer. The reason why the channel height of 0.4 and 0.7 gives slightly better heat transfer for *z/d* = 4 is that is how the geometry of the channels combined with the jet-to-target spacing's affected the heat transfer. In Figs. (5-7, 5-8, and 5-9), one can see clearly that the channel heights of 1.0, 1.4, 1.8 for *z/d* = 6 give better heat transfer results compared to *z/d* = 8 or

4. As a result z/d = 6 was selected as the optimum jet-to-target spacing for further parametric study.

Figure 5-6: Results for h/d = 0.7 for different z/d = 4, 6 & 8

Figure 5-7 shows the heat transfer distribution results of a fixed channel height of 1.0 at various jet-to-target spacings. The heat transfer results of the channel placed at 1.0 for a jet-to-target spacing of 6 gives a higher Nu_{avg} compared to z/d = 4, and 8. The heat transfer peaks at around x/s = 2 because of the channel inlet placement at around this point and then it starts to drop off gradually. An increase of approximately 20% is observed in Nu_{avg} for the channel height of 1.0 at z/d = 6 compared to other channel heights.

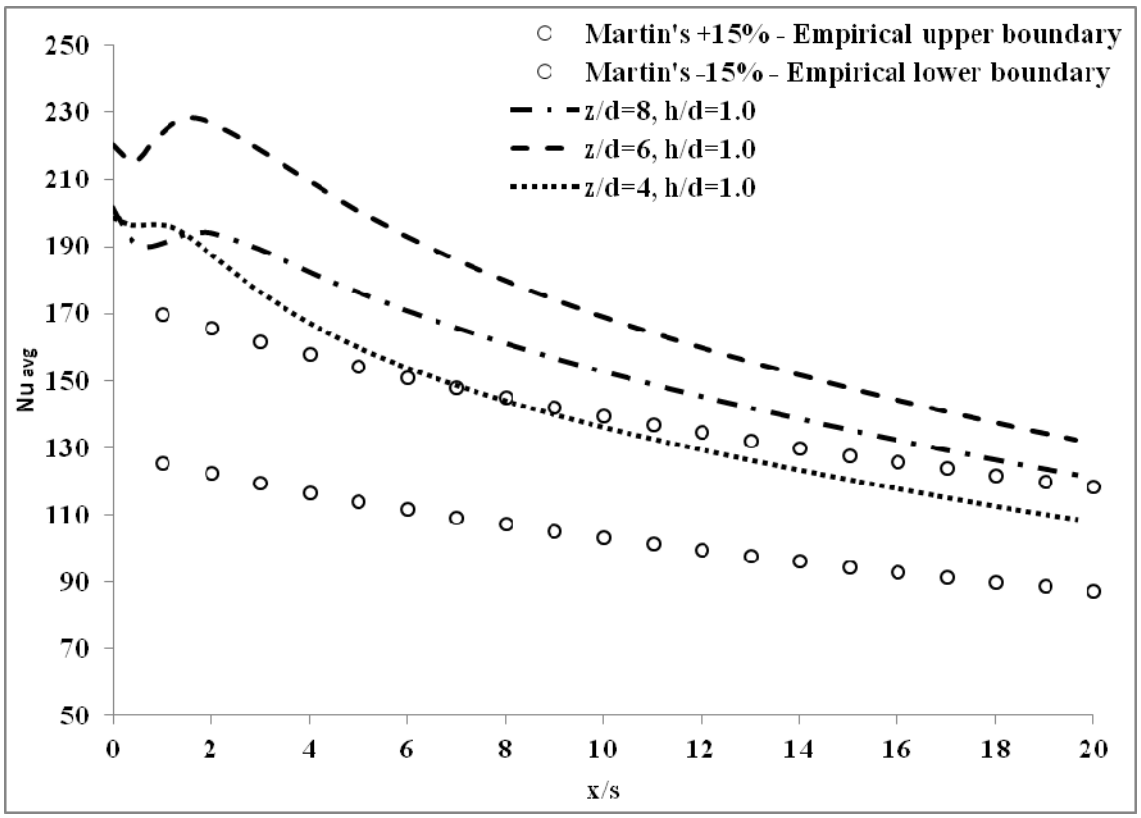

Figure 5-7: Results for *h/d* = 1.0 for different *z/d* = 4, 6 & 8

Figure 5-8 shows the results of a channel height of 1.4 for various jet-to-target spacings. The results here indicate that the heat transfer is more or less around the same Nu_{avg}, between 190-220. The jet-to-target spacing of 6 gives the maximum heat transfer compared to 4 and 8.

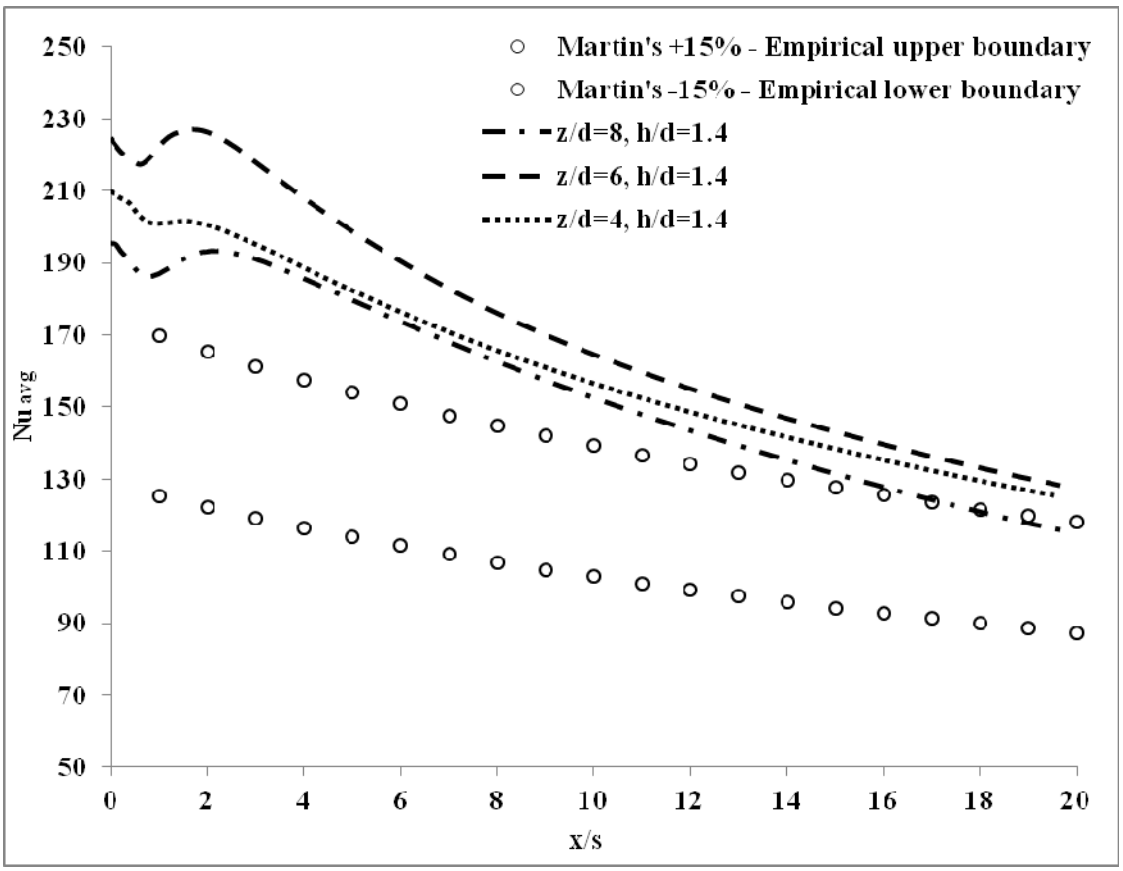

Figure 5-8: Results for *h/d* = 1.4 for different *z/d* = 8, 6 & 4

Figure 5-9 shows the results of channel height of 1.8 for various jet-to-target spacings. The channel at *z/d* = 6 gives the maximum heat transfer compared to the other jet-to-target spacing's. The peak at *x/s* = 2 for the channel placed at *z/d* = 6 is higher compared to the other channels because the shear stress on the wall for this channel was found to be very high compared to other channel heights and greater turbulence was also found compared to the channels placed at jet-to-target spacings of 4 and 8.

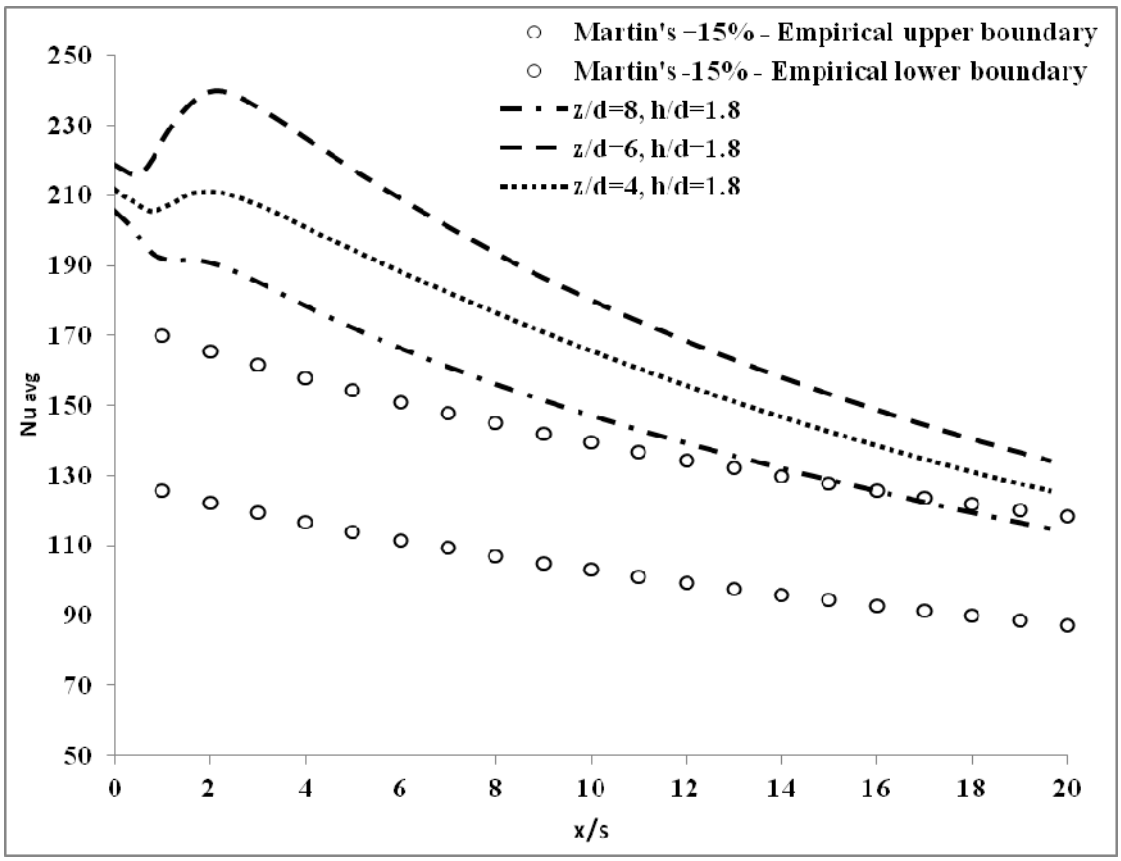

Figure 5-9: Results for *h/d* = 1.8 for different *z/d* = 4, 6 & 8

Figure 5-10 shows the results for the baseline model, i.e without any channel placed inside them for various jet-to-target spacings. The jet-to-target spacing at *z/d* = 6 gives marginally overall higher heat transfer distribution compared to 4 and 8. The difference in Nu_{avg} for the three cases *z/d* = 4, 6 and 8 is found to decrease with increasing *x/s* or as the flow moves away from the stagnation region.

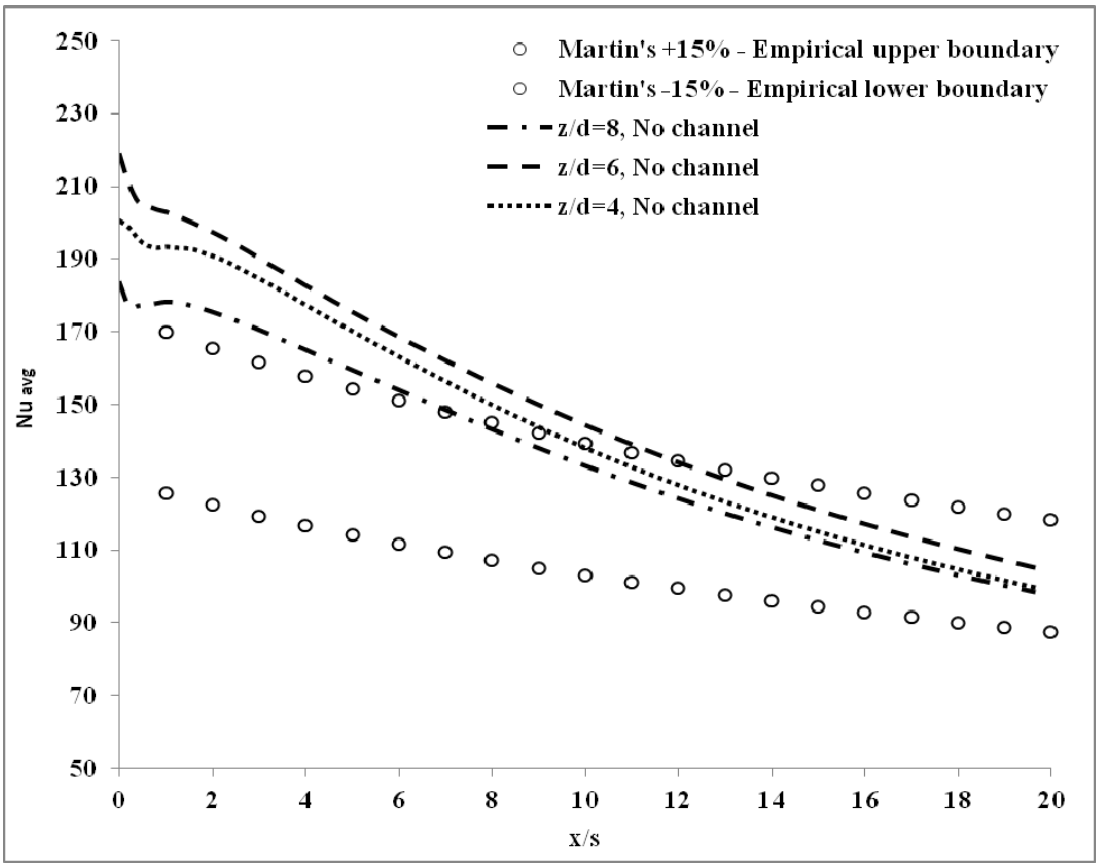

Figure 5-10: Baseline models at various *z/d* = 8, 6, 4

5.4 Effect of Jet Reynolds number

Next, the effect of Reynolds number on Nu_{avg} was studied. All the previous simulations were performed using Re = 60,000. To study the effect of Reynolds number the baseline case was studied at two additional Re of 30,000 and 90,000. This was done to understand how the change in Reynolds number affects the heat transfer on the impinging wall and inside the channels. Martins empirical correlation for flat plate were used at corresponding Re to compare with the numerical results it.

The numerical results at Re = 60,000 reveal that for smaller channel heights (*h/d* = 0.4 and 0.7) a smaller jet-to-target spacing gave better overall heat transfer. Likewise for higher channel heights (*h/d* = 1.0, 1.4 and 1.8) a higher jet-to-target spacing of *z/d* = 6 was found to give higher overall heat transfer distribution.

5.4.1 Effect of jet Reynolds number at 30,000

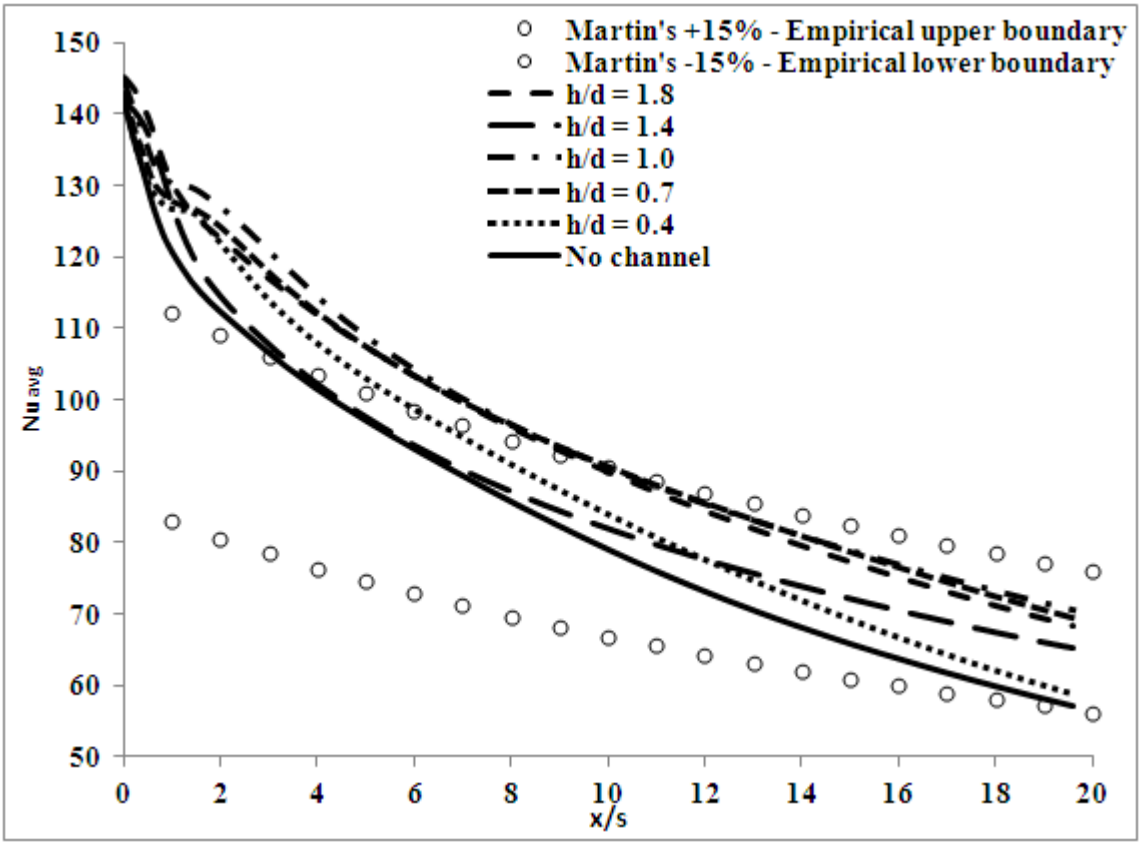

Figure 5-11: Results for *z/d* = 6 for Re = 30,000

Figure 5-11 shows the results for Re = 30,000. Compared to the previous simulations, here the heat transfer for all the channels are in very close proximity of each other making it difficult to point at a certain channel height to state that it gives the maximum however on close observation the channel at *h/d* = 1.0 gives a slightly higher heat transfer

compared to the other channels. At Re = 30,000 the overall heat transfer distribution is lowered by almost 66% compared to Re = 60,000. No peak at *x/s* = 2 is observed here compared to the other results.

5.4.2 Effect of jet Reynolds number at 60,000

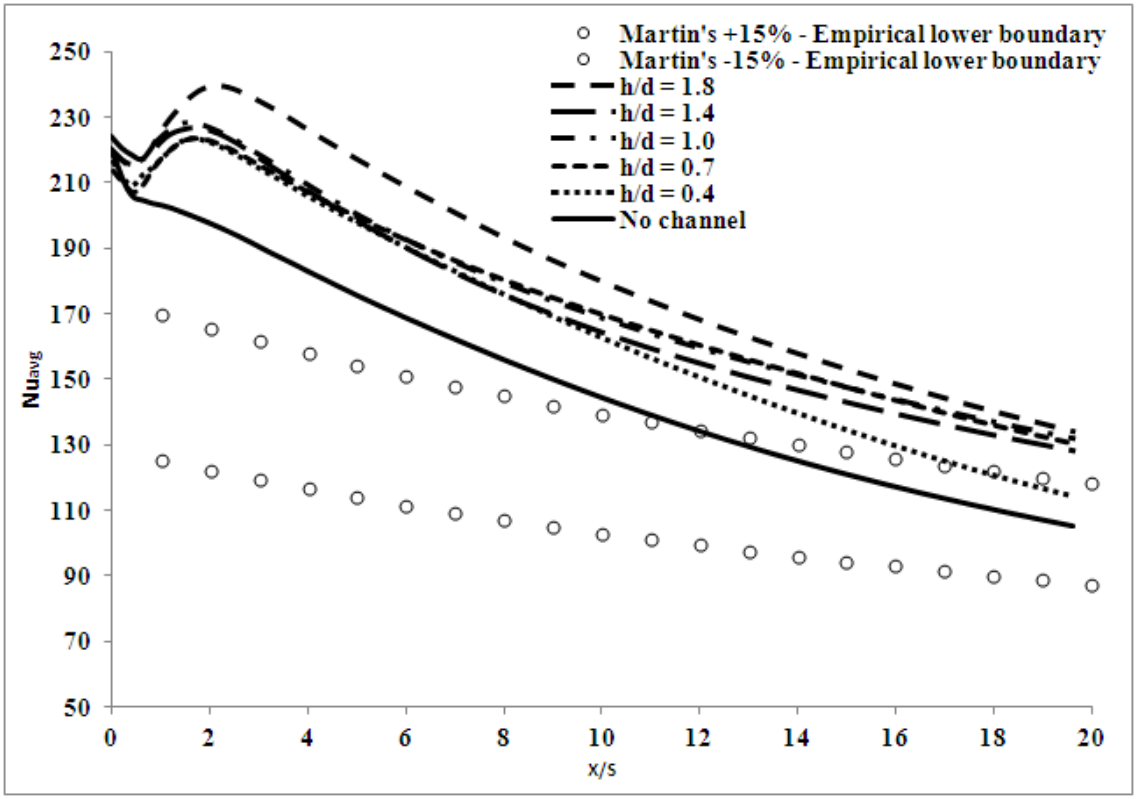

Figure 5-12: Results for *z/d* = 6 for Re = 60,000

Figure 5-12 shows the result at *z/d* = 6 for Re = 60,000. It gives an insight of the various channel heights *h/d*. The channel height of *h/d* = 1.8 gives the highest heat transfer distribution among all the other channel heights. The rest of the channels follow suit with heat transfer decreasing gradually. One important trend seen is the heat transfer increases just after the stagnation region and then starts to fall-off gradually, this is due to the shear stress at the wall and turbulence at *x/s* = 2 which corresponds to the placement of the

channel inlet. The baseline model for z/d = 6 also delivers higher heat transfer than the baseline model at z/d = 8 indicating that this jet-to-target spacing value can be highly capable of giving higher heat transfer. Although the heat transfer results at the channels give a higher value compared to the Martins spread, the baseline model falls within range at around x/s = 12.

5.4.3 Effect of jet Reynolds number at 90,000

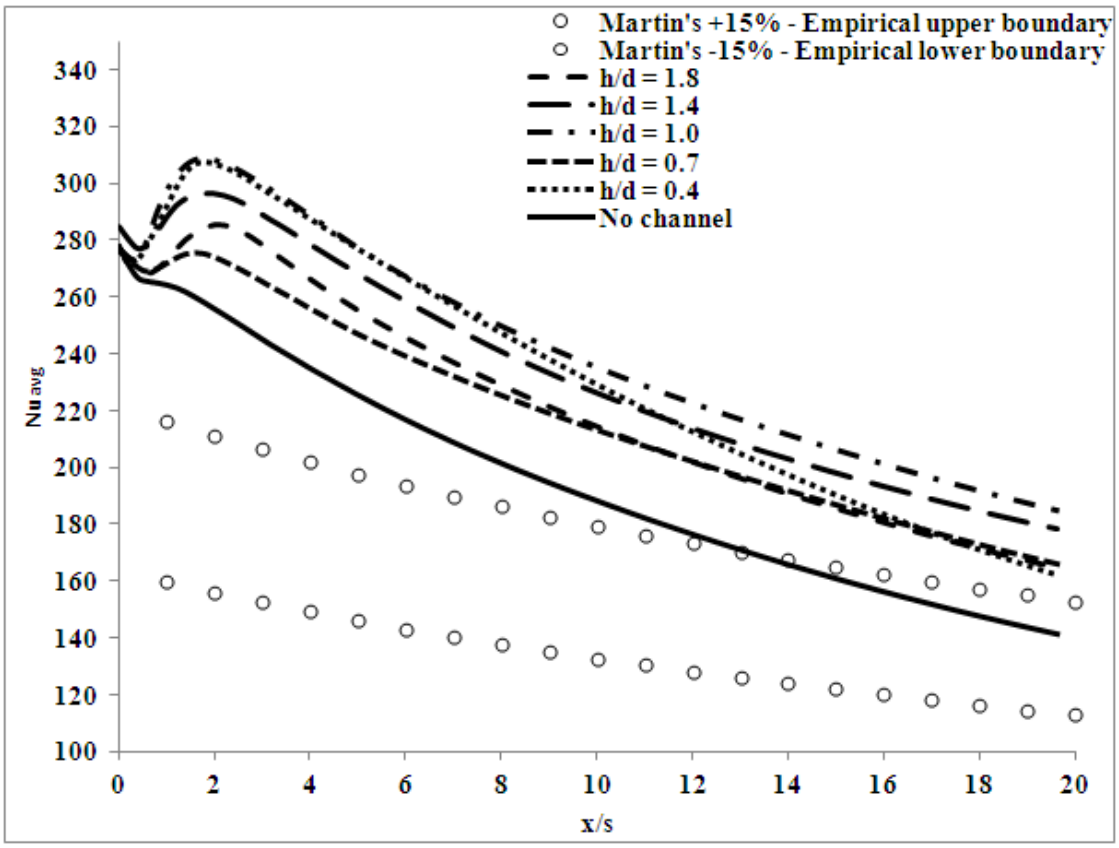

Figure 5-13: Results of z/d = 6 for Re = 90,000

Figure 5-13 shows the heat transfer distribution results at Re = 90,000. The channel height of 1.0 gives marginally higher heat transfer. As expected, increased heat transfer is

obtained with increasing Re. Moreover, the difference in Nu_{avg} between different channel heights is more pronounced.

5.5 Effect of channel inlet location angle θ

The channel inlet location angle was measured from the piccolo tube center and the chord line. The angles investigated were θ = 10°, 20°, 40° and 60°. The reason for this modeling and simulation was to first satisfy the objective of our study which was to find out which angle particularly gives the maximum heat transfer and suitable for the placement of the channel inlet. For this simulation a jet-to-target spacing of z/d = 6 and Reynolds number = 60,000 were used as in the baseline case. Martins data for Re = 60,000 was used as reference.

5.5.1 Effect of channel inlet location angle θ = 10°

Figure 5-14 shows the results for the channel inlet placement angle of 10° for various channel heights. The channel at h/d = 1.8 gives the maximum heat transfer. As seen with the previous results the heat transfer increases sharply just after the stagnation region at around x/s = 2 because of the channel inlet placement at this point causing the flow when entering into the channel to have turbulence and stresses on the wall of the liner and the impinging wall.

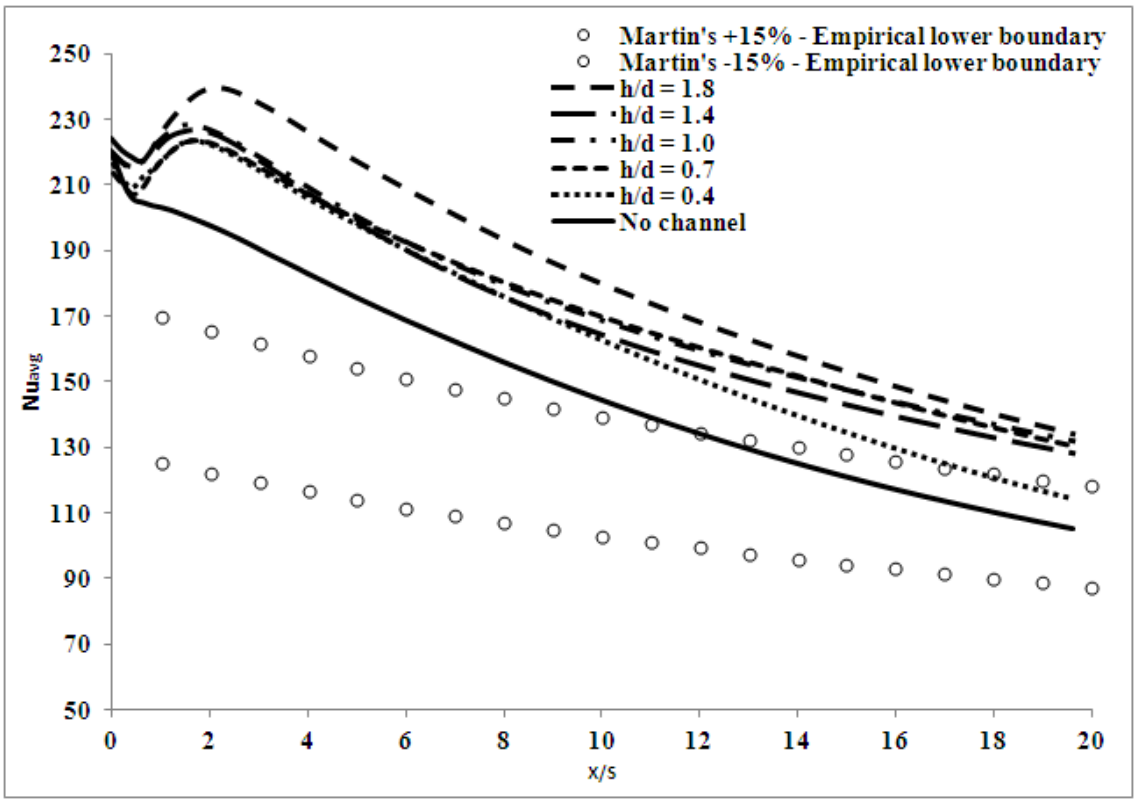

Figure 5-14: Effect of channel inlet location angle θ = 10° on heat transfer

5.5.2 Effect of channel inlet location angle θ = 20°

Figure 5-15 shows the results for inlet inclination angle θ = 20°. The overall heat transfer distribution is comparatively less than for θ = 10°. The reason behind the other channels not exhibiting a peak is there is not much turbulence at the channel inlet since it is placed at an angle further away from the jet inlet. The channel height of 0.7 provides higher heat transfer results compared to the other channels.

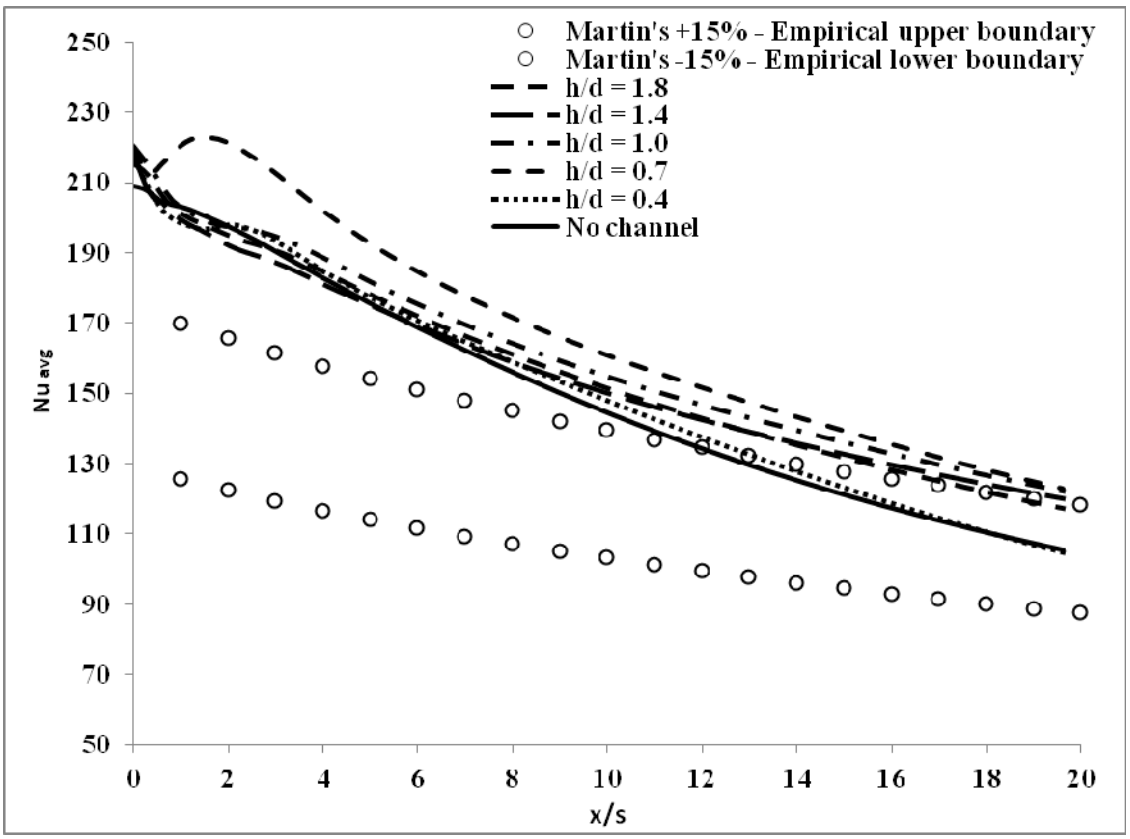

Figure 5-15: Effect of channel inlet location angle θ = 20° on heat transfer

5.5.3 Effect of channel inlet location angle θ = 40°

Figure 5-16 presents the heat transfer distribution results for inlet location angle of θ = 40°. The channel height of 1.8 gives highest heat transfer distribution compared to the other channels. No peak in heat transfer at *x/s* = 2 is observed here because the channels are placed farther away from the stagnation region. Another interesting thing is all the channels eventually enter into the Martins range at *x/s* = 19 and although there is initial difference of heat transfer between them, they all gradually come closer at *x/s* = 20.

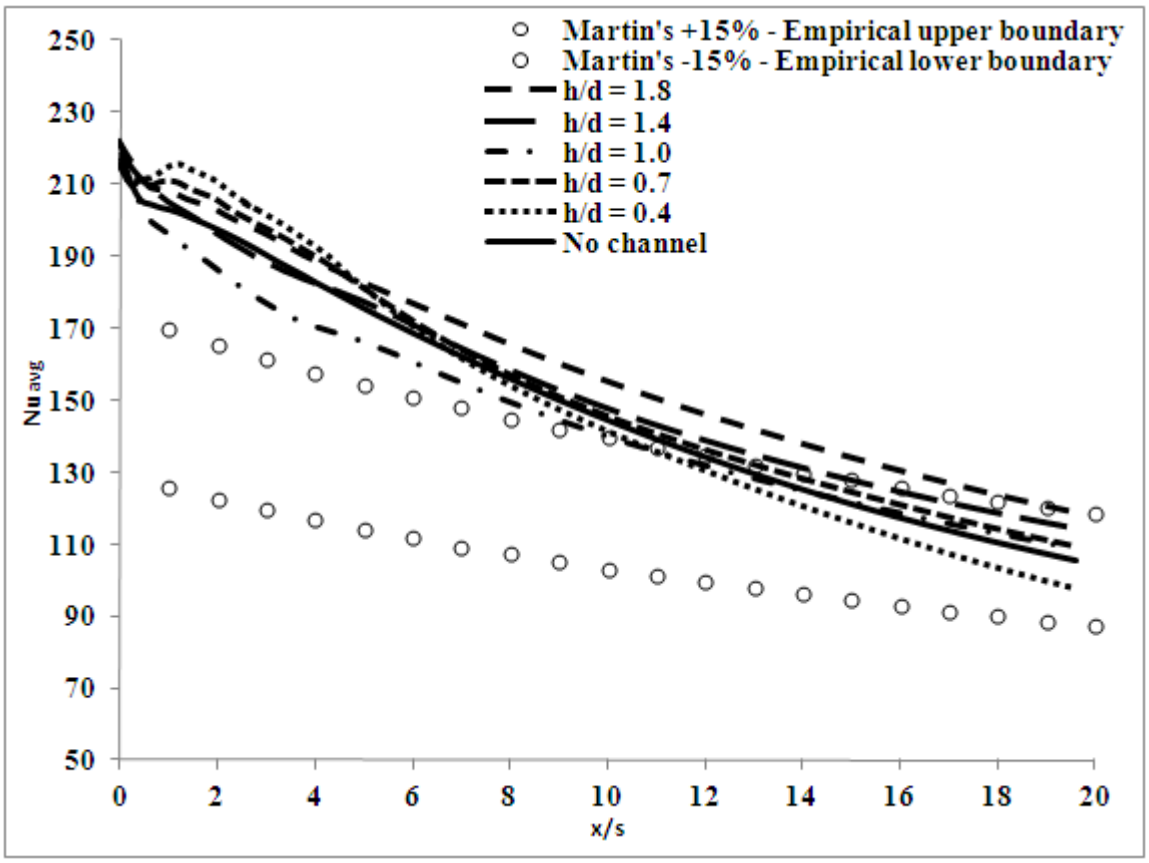

Figure 5-16: Effect of channel inlet location angle θ = 40° on heat transfer

5.5.4 Effect of channel inlet location angle θ = 60°

Figure 5-17 gives the results for inlet location angle of θ = 60°. The channel height of 0.7 gives a marginally higher average heat transfer distribution compared to the other channels. All of the channels move closely with each other in terms of heat transfer. There is no peak after the stagnation region and heat transfer continues to fall off gradually along the wall jet region. They fall into the Martin's spread of ± 15 % early on and move through it. This channel inlet placement angle gives the lowest overall heat transfer compared to all the other angles. This is because the angle of 60˚ is very high as a result the distance from the jet inlet to the channel inlet is greater indicating for

optimum heat transfer results the channels should be placed at a lower angle preferably at 10˚ or less.

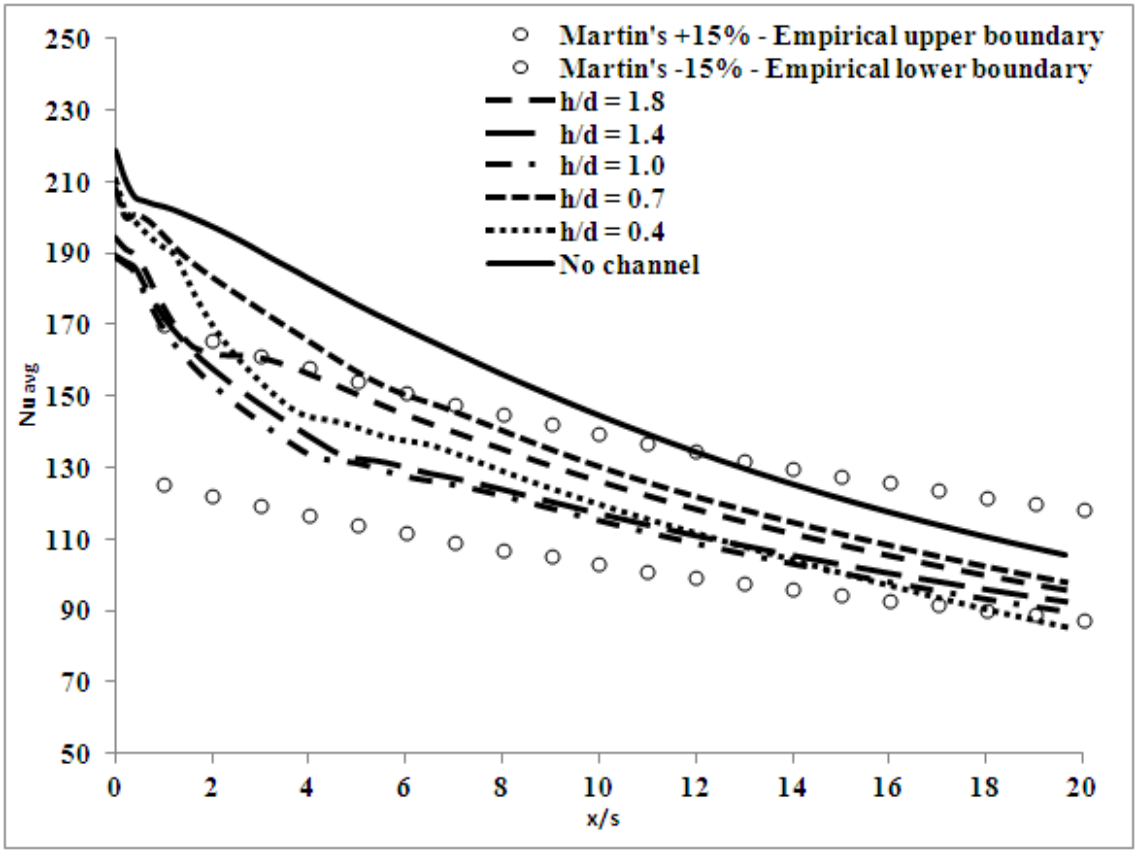

Figure 5-17: Effect of channel inlet location angle θ = 60° on heat transfer

5.6 Maximum average Nusselt number

The maximum average Nusselt number is the peak value or the absolute highest point value in the graph plotted for average Nusselt number distribution along the upper (positive) side of the curved model (see Fig. 5-18). Table 5-1 displays the value of the maximum peak point on the graph where heat transfer or Nu_{avg} is maximum in all the cases, studied.

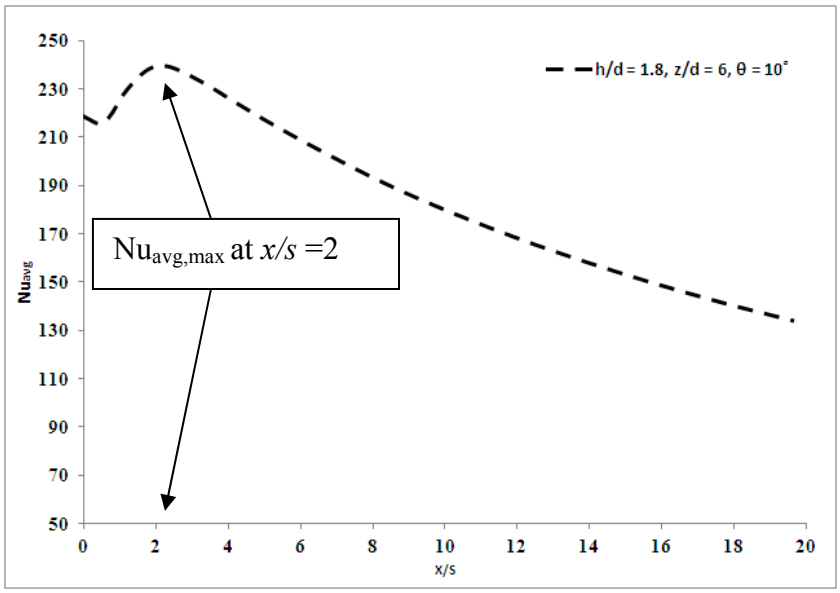

Figure 5-18: Example of documenting the Maximum Nusselt number from every graph.

The maximum Nu_{avg} = 308.64 is predicted for Case ID # 5C, where θ = 10˚, Re = 90,000, z/d = 6 and h/d = 1.0.

Table 5-1: Maximum Nu_{avg} values prediction for all the cases investigated

Case ID #	θ	Re	z/d	h/d						$Maximum\ Nu_{avg}$					
				A	B	C	D	E	F	A	B	C	D	E	F
1	10°	60,000	8	0.4	0.7	1.0	1.4	1.8	NC	197.05	201.70	201.57	195.29	205.56	183.28
2	10°	60,000	6	0.4	0.7	1.0	1.4	1.8	NC	223.50	223.41	228.59	226.82	239.68	218.61
3	10°	60,000	4	0.4	0.7	1.0	1.4	1.8	NC	228.32	226.82	198.65	210.03	211.67	215.58
4	10°	30,000	6	0.4	0.7	1.0	1.4	1.8	NC	142.11	142.83	144.48	141.78	145.10	141.53
5	10°	90,000	6	0.4	0.7	1.0	1.4	1.8	NC	307.25	276.94	308.64	296.15	285.46	277.50
6	20°	60,000	6	0.4	0.7	1.0	1.4	1.8	-	216.93	222.76	220.04	209.15	215.20	-
7	40°	60,000	6	0.4	0.7	1.0	1.4	1.8	-	214.48	217.04	215.94	221.49	221.94	-
8	60°	60,000	6	0.4	0.7	1.0	1.4	1.8	-	210.20	207.60	188.58	189.43	194.12	-

* NC = No Channel

5.7 Slope of average Nusselt number distribution

The slope of Nu_{avg} distribution is calculated using the peak (at x/s = 2) and final (at x/s = 20) values of Nu_{avg} as indicated in Fig. 5-19.

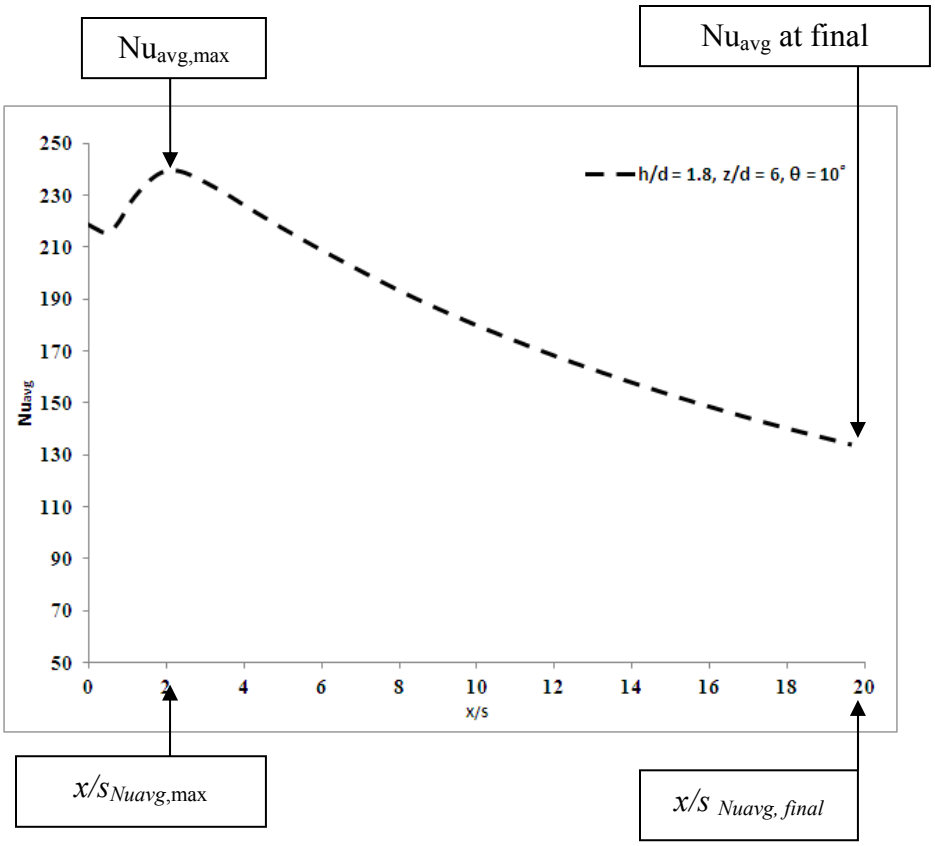

Figure 5-19: Example of calculating slope of Nu_{avg}

Mathematically this slope can be obtained from the relation:

$$\frac{dNu_{avg}}{d(x/s)} = \frac{Nu_{final} - Nu_{avg,max}}{20 - x/s_{Nuavg,max}} \tag{5.1}$$

where

$Nu_{avg,final}$ = Nusselt number at x/s = 20.

$Nu_{avg,max}$ = Maximum Nusselt number,

$x/s_{Nuavg,max}$ = Value of x/s at maximum Nusselt number.

Table 5-2 lists the slope of Nu_{avg} distribution for all the cases studied and indicates that Case ID # 4B with the configuration of $\theta = 10^{\circ}$, $z/d = 6$, Re = 30,000 and $h/d = 0.7$ yields the lowest value of this slope which can be interpreted as the case with lowest heat transfer. The case which gives the highest value of slope which can be interpreted as the case with the highest heat transfer is Case ID # 5A where $\theta = 10^{\circ}$, $z/d = 6$,Re = 90,000, and $h/d = 0.4$.

Table 5-2: Slope of Nu_{avg} distribution determined from numerical simulations

Case ID #	θ	Re	z/d	h/d						Slope of Nu_{avg} Distribution					
				A	B	C	D	E	F	A	B	C	D	E	F
1	10°	60,000	8	0.4	0.7	1.0	1.4	1.8	NC	-5.226	-4.555	-3.968	-3.959	-4.530	-4.231
2	10°	60,000	6	0.4	0.7	1.0	1.4	1.8	NC	-5.917	-5.101	-5.233	-5.344	-5.914	-5.666
3	10°	60,000	4	0.4	0.7	1.0	1.4	1.8	NC	-5.788	-4.958	-4.488	-4.242	-4.296	-5.405
4	10°	30,000	6	0.4	0.7	1.0	1.4	1.8	NC	-4.172	-3.676	-3.701	-3.823	-3.846	-4.217
5	10°	90,000	6	0.4	0.7	1.0	1.4	1.8	NC	-7.953	-5.534	-6.790	-6.468	-6.690	-6.815
6	20°	60,000	6	0.4	0.7	1.0	1.4	1.8	-	-5.618	-5.362	-4.885	-4.461	-4.900	-
7	40°	60,000	6	0.4	0.7	1.0	1.4	1.8	-	-5.843	-5.382	-5.365	-5.359	-5.156	-
8	60°	60,000	6	0.4	0.7	1.0	1.4	1.8	-	-6.247	-5.485	-4.932	-4.849	-4.907	-

* NC = No Channel

CHAPTER 6

CONCLUSIONS

The objective of the present investigation was to study the effect of various geometric parameters of a channel used to enhance heat transfer characteristics of a hot-air jet impingement on a curved wall that is maintained at a much cooler temperature (below the freezing point of water) to simulate a hot-air jet based anti-icing system. These geometric parameters are:

- The jet-to-target spacing *z/d*.
- The channel height *h/d*.
- The channel inlet location angle θ.
- The jet Reynolds number Re.

All the cases were modeled in GAMBIT and simulated in FLUENT, a commercial CFD code. The boundary conditions used in the cases were taken from the literature survey. The Spalart Allmaras turbulence model was used in all of simulations. Grid requirements

are set according to FLUENT guidelines. Grid convergence study was used to get optimum grids (about 350,000 cells). Each case took an average of 36 hours to converge with the convergence criteria for residuals set at 10^{-6}. A total of 48 numerical cases were run to study the effect of the above parameters.

Initially a flat-plate case was used to validate the numerical model with empirical correlations of Martin available in literature. The flat-plate numerical model results were found to be in good agreement with the empirical correlations. Next, the same model with all its dimensions and boundary conditions was transformed into a curved surface model with a NACA 23012 leading edge profile. The curved surface results showed an increase in heat transfer characteristics in terms of average Nusselt number (Nu_{avg}) by approximately 10%, which is due to the fact that heat transfer rate for impingement on curved surfaces increases by as much as 20% as reported by Sharif and Mothe [42]. The curvature was seen to impart more momentum to the wall jet which resulted in an increase in heat transfer. Then, the case of the curved wall model with a channel placed inside it was analyzed and a baseline curved model was established. The results for the curved model with a channel results in a further increase in heat transfer up to 20% compared to the curved model without the channel and significantly more compared to the flat plate model.

A summary of important findings of this study are as follows:

6.1 Effect of jet-to-target spacing *z/d*

The effect of jet-to-target spacing *z/d* on Nu_{avg} on the impingement wall was studied for *z/d* values of 4, 6, and 8 values. For each case, five different channel heights (*h/d* = 0.4,

0.7, 1.0, 1.4, and 1.8) were simulated at a channel inlet angle of $\theta = 10°$ and Re = 60,000. A case without channel was also simulated for comparison. The results reveal that the channel height and jet-to-target spacing have a direct relation with the heat transfer and as the jet-to-target spacing was varied heat transfer results also varied. Among the cases investigated, the jet-to-target spacing of 6 gave the highest overall heat transfer distribution.

6.2 Effect of channel height *h/d*

The effect of channel height on Nu_{avg} was studied for h/d = 0.4, 0.7, 1.0, 1.4, and 1.8. Since highest overall heat transfer distribution was found for a jet-to-target spacing z/d of 6, the simulations to study the effect of channel height were performed at $z/d = 6$, $\theta = 10°$ and Re = 60,000. The numerical results revealed that for smaller channel heights (h/d = 0.4 and 0.7) a smaller jet-to-target spacing gave better overall heat transfer. Likewise for higher channel heights (h/d = 1.0, 1.4 and 1.8) a higher jet-to-target spacing of $z/d = 6$ was found to give higher overall heat transfer distribution. The results show that the value of $h/d = 1.8$ gave the highest overall heat transfer distribution as compared to the other channel heights considered. A further investigation should look at $h/d > 1.8$ to determine the optimum h/d.

6.3 Effect of channel inlet location angle θ

The effect of channel inlet location angle on Nu_{avg} was studied for θ values of 10°, 20°, 40° and 60°. Out of the 4 channel inlet location angles investigated the inlet location angle 10° gave the highest overall heat transfer distribution. A further investigation should look at $\theta < 10°$ to determine the optimum θ. The results suggest that the channel

should be placed near the stagnation region as close as possible. All the angles were investigated at a jet-to-target spacing *z/d* of 6 since it gave the highest overall heat transfer distribution. It was observed as the channel inlet location angle was increased the heat transfer decreased. This is due to the fact that as the distance of the channel inlet increases from the stagnation region, the flow and its momentum entering the channel decreases.

6.4 Effect of jet Reynolds Number

The effect of jet Reynolds number on Nu_{avg} was studied for Re values of 30,000 and 90,000. This was done to understand how the change in Reynolds number affects the heat transfer on the impinging wall and inside the channels. Martins empirical correlation for flat plate for Re = 30,000 and 90,000 were used for comparison. The result showed that by increasing the Reynolds number, the overall heat transfer distribution increased substantially.

6.5 Recommendations

The present investigation was limited to fewer parameters and parametric changes. Although important findings were made, there are still unanswered questions such as:

- What is the optimum channel height? Although *h/d* = 1.8 gave highest heat transfer results, cases need to be done by increasing *h/d* greater than 1.8 to find its effect on heat transfer.

- What is the optimum θ? Cases need to be done by varying the angle above and below 10° to observe its effect on heat transfer.

- What is the effect of a combination of channel and other surface obstructions?
- How 3D modeling of the above cases will affect heat transfer results of channels placed inside the leading edge?

REFERENCES

[1] Cessna 208B Caravan. In wikepedia. Retreived on March 2012 from http://en.wikipedia.org/wiki/Cessna_208_Caravan

[2] Cuban authorities investigate crash of cuban airliners, 2010, Retrieved on March 2012 from www.canadiannetworkoncuba.com

[3] AOPA Air Safety Foundation, Safety Advisor, "Aircraft Icing" Retrieved on March 2012 from http://www.aopa.org/asf/publications/sa11.pdf#search=%22anti-icing%20systems%20aircraft%22

[4] Department of Aerospace and Oceanic Engineering department, Virginia Tech University, "Anti-Icing" , Retrieved from www.dept.aoe.vt.edu/~mason/Mason_f/AntiIcingT4.ppt

[5] Lee, S, and Bragg, M.B., "Experimental Investigation of Simulated Large-Droplet Ice Shapes on Airfoil Aerodynamics". AIAA *Journal of Aircraft*, Vol. 36, No. 5, 1999, pp. 844–850.

[6] Lee, S, and Bragg, M.B., "Investigation of Factors Affecting Iced-Airfoil Aerodynamics". AIAA *Journal of Aircraft* Vol. 40, No. 3, 2003, pp. 499–508.

[7] Olsen, W, R. and Shaw, J. N., "Ice Shapes and the Resulting Drag Increase for a NACA 0012 Airfoil." NASA Technical Report 83556, 1984.

[8] Reehorst, A., L., Chung J., Potapczukn M., and Cho, Y., "Study of Icing Effects on Performance and Controllability of an Accident Aircraft". AIAA *Journal of*

Aircraft, 2000, pp. 253–259

[9] Federal Aviation Administration, *Proceeding of the FAA International Conference on Aircraft In-Flight Icing*, Vol. I and II, Springfield, Virginia, May 6—8, 1996. Final Report.

[10] United States Department of Transportation, Federal Aviation Administration. FAA In-Flight Icing Plan, Apr. 1997.

[11] National Transportation Safety Board, Retrieved on March 2012, http://www.ntsb.gov/aviation/aviation.htm

[12] Thomas, S. K., Cassoni, R. P., and MacArthur, C. D., "Aircraft Anti-Icing and Deicing Techniques and Modeling," AIAA *Journal of Aircraft*, Vol. 33, No. 5, Sept.-Oct. 1996, pp. 841—854.

[13] Cornaro, C., Fleischer, A. S., and Goldstein, R. J., "Flow Visualization of a Round Jet Impinging on Cylindrical Surfaces," *Experimental Thermal and Fluid Science*, Vol. 20, 1999, pp. 66—78.

[14] Metzger, D. E., Yamashita, T., and Jenkins, C. W., "Impingement Cooling of Concave Surfaces with High Velocity Impinging Air Jets," *Journal of Engineering for Power-Transactions of the ASME*, Vol. 91, 1969, pp. 149—158.

[15] Dyban, E. P., and Mazur, A. I., "Heat Transfer for a Planar Jet Striking a Concave Surface," translated from *Inzhenerno-Fizicheskii Zhurnal*, Vol. 17, No. 5, Nov. 1969, pp. 785—790.

[16] Al-Khalil, K. M., *Numerical Simulation of an Aircraft Anti-Icing System Incorporating a Rivulet Model for the Runback Water*, Ph.D. thesis, University of Toledo, Ohio, USA, June1991.

[17] Al-Khalil, K. M., and Potapczuk, M. G., "Numerical Modeling of Anti-Icing Systems and Numerical Comparison to Test Results on a NACA 0012 Airfoil," 31st Aerospace Sciences Meeting & Exhibit, AIAA Paper 93-0170, Reno, NV, Jan.1993.

[18] Martin, H., "Heat and Mass Transfer between Impinging Gas Jets and Solid Surfaces," *Advances in Heat Transfer*, Vol. 13, Academic Press, 1977, pp. 1—60.

[19] Jambunathan, K., Lai, E., Moss, M. A., and Button, B. L., "A Review of Heat Transfer Data for Singular Jet Impingement," *International Journal of Heat and Fluid Flow*, Vol. 13, 1992, pp. 106—115.

[20] Zhou, D., Lee, S. J., Ma, C. F. & Bergles, A. E., "Optimization of Mesh Screen for Enhancing Jet Impingement Heat Transfer," *Heat and Mass Transfer*, Vol. 42, 2006, pp. 501—510.

[21] Papadakis M., Wong S.H.J "Parametric Investigation of Bleed Air Protection System," 44th AIAA Aerospace Sciences Meetings and Exhibit, 2006, pp. 9 – 12.

[22] Saeed, F., and Al-Garni, A.Z., "Numerical Simulation of Surface Heat Transfer from an Array of Hot-air Jets," 25th AIAA Applied Aerodynamic Conference, 2007, pp. 25—28.

[23] Zhou, D.W., and Lee, S.J., "Forced Convective Heat Transfer with Impinging Rectangular Jets" *International Journal of Heat and Mass Transfer*, 2007, pp. 1917—1926.

[24] Lee, D.H., Lee, Y.M., Kim, Y.T., Won, S.Y. and Chung, Y.S., "Heat Transfer Enhancement by the Perforated Plate Installed between an Impinging Jet and the Target Plate," *International Journal of Heat and Mass Transfer*, Vol. 45, 2002, pp.

213—217.

[25] Haneda, Y., Tsuchiya, Y., Nakabe, K. and Suzuki, K., "Enhancement of Impinging Jet Heat Transfer by making use of Mechano-Fluid Interactive Flow Oscillation," *International Journal of Heat and Fluid Flow*, Vol. 19, 1998, pp. 115—124.

[26] Bergles. E, "Heat Transfer Enhancement - The Maturing of Second-Generation Heat Transfer Technology," *Heat Transfer Engineering,* Vol 1, Issue 1, 1997, pp. 47—55.

[27] Gardon, R., Akfirat, J. C., "The Role of Turbulence in Determining the Heat Transfer Characteristics of Impinging Jets," *International Journal of Heat Mass Transfer*, Vol. 8, 1965, pp. 1261—1272.

[28] Obot, N. T., Majumdar, A. S., and Douglas, W. J. M., "The Effect of Nozzle Geometry on Impingement Heat Transfer under a Round Turbulent jet," ASME Paper No.79-WA/HT-53, 1979.

[29] Popiel, C. O., and Boguslawski, L., "Effect of Flow Structure on the Heat or Mass Transfer on a Flat Plate in Impinging Round Jet", in: Proc. 2nd UK National Conference on Heat Transfer, University of Strathclyde, Vol. 1, 1988, pp. 663—685.

[30] Oyakawa, K., Azama, T., Senaha, I., and Hiwada, M., "Effects of Nozzle Configuration on Impingement Heat Transfer", in: Proc. ASME/JSME Thermal Engineering Conference, Maui, USA, Vol. 1, 1995, pp. 377—384.

[31] Zumbrunnen, D. A., and Aziz, M., "Convective Heat Transfer Enhancement Due to Intermittency in an Impinging Jet," *Journal of Heat Transfer*, Vol. 115, Feb. 1993, pp. 91- 98.

[32] Tawfek A. A., "Heat Transfer and Pressure Distributions of an Impinging Jet on a Flat Surface" *Journal of Heat and Mass Transfer Volume 32*, Numbers 1-2, 49-54, Springer – Verlag, 1996.

[33] Saeed, F., Morency, F., and Paraschivoiu, I., "Numerical Simulation of a Hot-Air Anti- Icing Simulation," 38th Aerospace Sciences Meeting & Exhibit, AIAA Paper 2000-0630, Reno, NV, Jan. 2000.

[34] Saeed, F., and Paraschivoiu, I., "Numerical Correlation for Local Nusselt Number Distribution for Hot-Air Jet Impingement on Concave Surfaces," Proceedings of the 8th Annual Conference of the CFD Society of Canada, CFD2K, Montréal, Québec, Canada, June 11—13, 2000, Vol. 2, pp. 897—904.

[35] Fregeau, M., Saeed, F., and Paraschivoiu, I., "Numerical Heat Transfer Correlation for Array of Hot-Air Jets Impinging on 3-Dimensional Concave Surface," *AIAA Journal of Aircraft*, Vol. 42, No. 3, 2005, pp. 665—670.

[36] Brown, J. M., Raghunathan, S., Watterson, J. K., Linton, A. J., and Riordon, D., "Heat Transfer Correlation for Anti-Icing Systems," *AIAA Journal of Aircraft*, Vol. 39, No. 1, Jan-Feb 2002, pp. 65-70.

[37] Patel, P., and Roy, S., "Heat Transfer for a Pair of Rectangular Jets Impinging upon an Inclined Surface," 40th Aerospace Sciences Meeting & Exhibit, AIAA Paper 2002-0210, Reno, Nevada, Jan 2002.

[38] Hofmann, H., Martin, H., and Kind, M., "Numerical Simulation of Heat Transfer from an Impinging Jet to a Flat Plate," *Chemic Ingenieur Technik*, Vol 27, No.1, 2004, pp. 27-30.

[39] Schlunder, E.-U, and Gnielinski, V., Chem. Ing. Tech. 1967, 9/10, 578.

[40] Sarghini, F., and Ruocco, G., "Enhancement and Reversal Heat Transfer by Competing Modes in Jet Impingement," *International Journal of Heat and Mass Transfer*, Vol. 47, 2004, pp. 1711—1718.

[41] P. S. Shadlesky, "Stagnation Point Heat Transfer for Jet Impingement to a Plane Surface," *AIAA Journal*, Vol. 21, No. 8, 1982, pp. 1214—1215.

[42] Sharif, M.A.R., and Mothe, K.K., "Parametric Study Of Turbulent Slot-Jet Impingement Heat Transfer From Concave Cylindrical Surfaces," *International Journal of Thermal Sciences*, Elsevier Masson SAS, July 2009.

[43] Korichi, A., Oufer, L., and Polidori, G., "Heat Transfer Enhancement in Self-Sustained Oscillatory Flow in a Grooved Channel with Oblique Plates", *International Journal of Heat and Mass Transfer*, Vol 52, 2009, pp. 1138—1148.

[44] Saeed, F., Al-Garni, A.Z., Khan Mohammed M.A., "Numerical Investigation Of Mechanisms To Aid In Enhancing Surface Heat Transfer From An Impinging 2D Hot-Air Jet," Canadian Aeronautics and Space Institute AERO'09 Conference Aerodynamics Symposium, 2009.

[45] Khan, M. M. A., "Numerical Investigation of Mechanisms to aid in Enhancing Surface Heat Transfer from an Impinging 2D Hot-Air Jet", Master Thesis, King Fahd University of Petroleum and Minerals, Jan 2010.

[46] Spalart, P., and Allmaras, S., "A One-Equation Turbulence Model for Aerodynamic Flows," Technical Report AIAA-92-0439, American Institute of Aeronautics and Astronautics, 1992.

[47] Wilcox, D. C., *Turbulence Modeling for CFD*, DCW Industries, Inc., La Canada, California, 1998.

[48] Livingood, J.N.B., and Hyrcak, P., “Impingement Heat Transfer From Turbulent Air Jets to Flat Plates - A Literature Survey” Lewis Research Center, NASA, Washington, May 1973.

VITAE

- Kamran Zaki Ahmed
- Contact Address: D'souza Mansion, Flat No.9, 2nd Floor, Nehru Rd, Santacruz, Mumbai, India
- Contact # +91 – 9870147508
- E-mail Address: ikamranz@yahoo.com
- Born on 7th May, 1986 in Mumbai, India
- Received Bachelor of Technology (B.Tech) degree in Aeronautical Engineering from J.R.N Rajasthan Vidyapeeth University , Rajasthan, India in November 2007
- Graduated from Department of Aerospace Engineering at King Fahd University of Petroleum and Minerals (KFUPM), Dhahran, Saudi Arabia in April 2012